Previsioni stagionali e proiezioni climatiche per la gestione della domanda irrigua territoriale in Emilia-Romagna

Andrea Gallo[1], Fausto Tomei[2], Giulia Villani[3], William Pratizzoli[2], Andrea Spisni[2], Vittorio Marletto[2]*

Abstract: *This paper describes the operative chain developed at Arpa-Simc based on the Criteria model, the regional soil use data and the operative seasonal forecasts and mid-term climate change projections, in order to improve the irrigation management in agriculture for Emilia-Romagna region.*
The remote sensing associated with field surveys is used to map the crops at the beginning of the irrigation season; the territorial water balance model, Criteria Geo, uses the crop map with the soil map and the weather data in order to simulate the soil water content. The weather data can be different: summer seasonal forecasts, that are used to forecast the irrigation water needs of crops for the 3-month period of June, July and August, or climate change scenarios for the 2021-2050 period with respect to 1961-1990, in order to evaluate the climate change impacts on future water needs of crops. The results of the application of the operative chain for the seasonal predictions referred to the summer 2010 and the results about the analysis of the climate change impacts for two regional case studies are described.
Keywords: *water balance, irrigation, Criteria, remote sensing.*

Riassunto: *Questo lavoro descrive la catena operativa sviluppata presso Arpa-Simc e basata sul modello di bilancio idrico Criteria, sull'utilizzo dei dati regionali di uso del suolo rilevati da satellite e su previsioni stagionali operative e proiezioni di cambiamento climatico a medio termine, al fine di migliorare la gestione delle risorse idriche in agricoltura per la regione Emilia-Romagna.*
Il telerilevamento affiancato da rilievi a terra viene utilizzato per mappare le colture all'inizio della stagione irrigua; il modello di bilancio idrico territoriale Criteria Geo utilizza quindi la mappa delle colture insieme alla carta dei suoli e ai dati meteo per simulare lo stato idrico dei suoli. I dati meteo possono essere di differente natura: previsioni stagionali estive che sono poi utilizzate per prevedere le necessità di irrigazione delle colture per il trimestre giugno-luglio-agosto o scenari di cambiamento climatico per il periodo 2021-2050 rispetto al clima 1961-1990, per valutare l'impatto del cambiamento climatico sui futuri fabbisogni irrigui delle colture. Vengono presentati i risultati dell'applicazione alla catena operativa delle previsioni stagionali per l'estate 2010 e quelli riguardanti lo studio dell'impatto del cambiamento climatico per due casi di studio regionali.
Parole chiave: *bilancio idrico, irrigazione, Criteria, telerilevamento.*

INTRODUZIONE

La razionalizzazione dell'uso della risorsa idrica in agricoltura è fondamentale, sia a livello globale che nelle aree del bacino del Mediterraneo nelle quali il verificarsi di annate siccitose è causa di conflitti tra i principali impieghi dell'acqua (Ragab e Prudhomme, 2002). In condizioni di siccità, infatti, viene data la priorità all'utilizzo idropotabile, penalizzando così gli altri possibili usi. In casi estremi diminuisce la disponibilità della risorsa idrica per gli usi agricoli durante il periodo primaverile-estivo che corrisponde a quello irriguo, creando gravi problemi al settore. Tutto ciò si può riscontrare anche in una regione come l'Emilia-Romagna, caratterizzata da una notevole produttività del settore agricolo e zootecnico.

I cambiamenti climatici in atto sia a livello globale (IPCC, 2007) che locale (Marletto *et al.*, 2010), impongono necessariamente un ripensamento nella politica di gestione della risorsa idrica, in particolar modo per l'agricoltura di tipo irriguo, che è condizionata in maggior misura dai prelievi idrici. Per questo motivo la regione Emilia-Romagna nel 2004 ha adottato il Piano di Tutela delle Acque (PTA) che definisce gli strumenti di pianificazione necessari al raggiungimento degli obiettivi di qualità delle risorse e dei corpi idrici fissati dalle normative italiane codificati in particolare nel Decreto Legislativo 152/99 in ottemperanza alle direttive dell'Unione Europea.

Tra gli interventi previsti dalla legislazione per il

* Corresponding Author:
Vittorio Marletto e-mail: vmarletto@arpa.emr.it
[1] Dipartimento di Economia e Sistemi Arborei, Sassari
[2] Arpa Servizio Idro-Meteo-Clima, Emilia-Romagna, Bologna, Italy
[3] DEIAGRA, Dipartimento di Economia ed Ingegneria Agrarie, Bologna, Italy
Received 30 November 2011, accepted 09 February 2012.

settore irriguo è contemplata l'elaborazione e la diffusione alle aziende agricole di un bilancio idrico aziendale in tempo reale. Attualmente, in molte aziende, infatti, il momento in cui irrigare e i volumi irrigui da impiegare vengono stabiliti in base a osservazioni empiriche relative alle condizioni delle colture e del terreno. Tali osservazioni portano spesso all'impiego di volumi di acqua eccessivi e in momenti non appropriati. Ne consegue che è quanto mai necessario un corretto impiego dei volumi di adacquamento sia da un punto di vista quantitativo che temporale: è possibile raggiungere tale obiettivo mediante il calcolo di un bilancio idrico che permette una valutazione del volume d'acqua necessario a colmare la differenza tra i consumi idrici delle colture per evapotraspirazione e gli apporti idrici dalle precipitazioni e dalle falde considerando anche le variazioni dei consumi irrigui delle colture durante le varie fasi di sviluppo vegetativo. Un esempio di questo tipo di applicazione pratica dei bilanci idrici è il sistema emiliano-romagnolo di consiglio irriguo aziendale Irrinet, al quale Arpa-Simc partecipa con i dati e le previsioni meteo (*http://irrigation.altavia.eu/logincer.aspx*).

Alla luce di queste considerazioni, i modelli di bilancio idrico e sviluppo colturale hanno un ruolo strategico poiché possono essere messi al servizio sia di realtà aziendali che di aree più estese come strumento decisionale.

Se nel primo caso i modelli di bilancio idrico sono di tipo puntuale, nel secondo caso essi devono essere integrati con strumenti che operano a dimensione territoriale come ad esempio il telerilevamento, grazie al quale è possibile individuare coperture colturali per aree estese.

Conoscere la distribuzione delle colture agricole ha una notevole importanza nella pianificazione delle risorse idriche, poiché permette di stimare il reale fabbisogno irriguo di un territorio tramite opportuni modelli di simulazione. A ciò si aggiunga che la modellistica può essere affiancata da prodotti climatologici come le previsioni stagionali o proiezioni di cambiamento climatico a medio o lungo termine; coniugare modello e previsioni stagionali consente, ad esempio, di valutare i volumi irrigui all'inizio della stagione estiva, che è quella che presenta maggiori criticità ed è soggetta a emergenze idriche indotte da siccità. In sintesi, valutare i fabbisogni irrigui delle colture ad un orizzonte temporale stagionale, significa essere in grado di razionalizzare e suddividere scientemente la risorsa tra i differenti impieghi. L'utilizzo poi di proiezioni di cambiamento climatico a lungo periodo nel modello di bilancio idrico amplia l'orizzonte temporale dell'analisi, consentendo una valutazione a lungo termine delle conseguenze del cambiamento climatico sul ciclo vegetativo delle colture e sull'irrigazione: valutazioni di questo genere possono essere strategiche al fine di applicare politiche di adattamento al cambiamento climatico.

L'intento di questo articolo, quindi, è quello di illustrare gli strumenti metodologici messi a punto da Arpa-Simc, integrati con previsioni stagionali e proiezioni di cambiamento climatico e alcuni dei risultati ottenuti all'interno dei progetti Colt 2010 e Agroscenari, mostrando le opportunità che tali strumenti presentano se utilizzati come mezzi decisionali e di gestione della risorsa idrica.

MATERIALI E METODI

Il modello Criteria

Criteria (Controllo delle Risorse Idriche Territoriali per la Riduzione dell'Impatto Ambientale) è un modello di bilancio idrico dei suoli di pianura e crescita colturale sviluppato da Arpa-Simc (Marletto *et al.*, 2007) che considera i principali processi che intervengono nel determinare il contenuto idrico di un suolo, schematizzati in Fig. 1.

Criteria è disponibile in due versioni: Criteria Banco di Prova (per analisi puntuali) e Criteria Geo (per analisi territoriali). Entrambe le versioni consentono di stimare:

– il volume d'acqua consigliato per l'irrigazione nel periodo di interesse e per una determinata area;

– il momento più opportuno nel quale procedere all'irrigazione delle colture.

Per poter effettuare queste stime, il modello utilizza in ingresso dati meteorologici giornalieri di temperatura e precipitazione, pedologici e agronomici che, per Criteria Geo, devono essere opportunamente georeferenziati (superfici delle colture da telerilevamento).

In particolare, per quanto riguarda la determinazione della domanda idrica, il processo di irrigazione è regolato attraverso l'inserimento di parametri quali la durata della stagione irrigua, il periodo minimo del turno irriguo, il volume massimo consentito per ogni singola irrigazione, il coefficiente colturale che la coltura raggiunge nel momento del massimo sviluppo, valori di sensibilità della pianta allo stress idrico ed eventuale percentuale di stress controllato.

La durata della stagione irrigua può essere inserita sia in forma di giorno dell'anno di inizio e fine della stessa sia in forma di sommatoria gradi giorno corrispondenti (soluzione, questa, più adatta ad un ap-

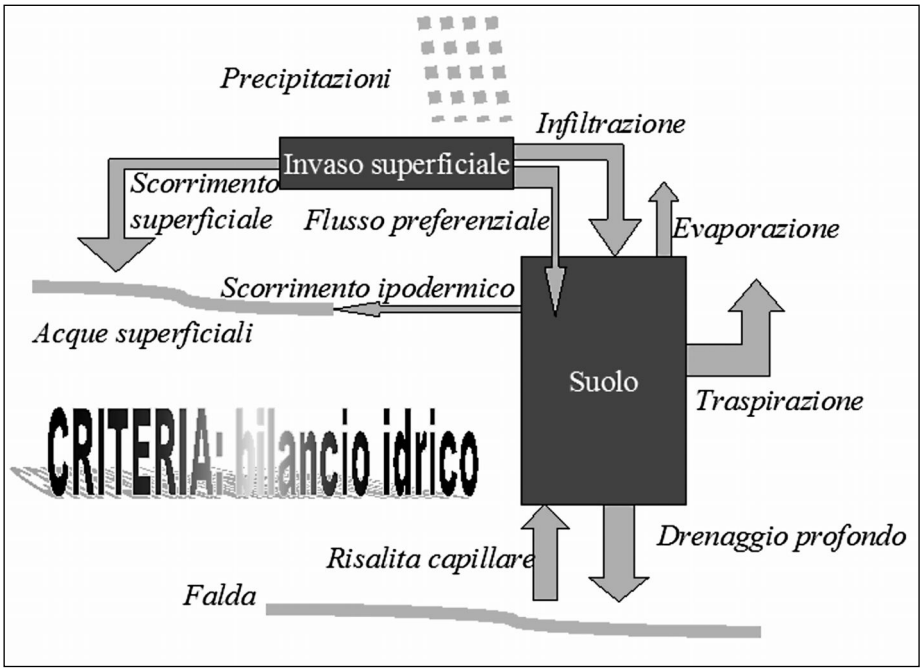

Fig. 1 - Schema del bilancio idrico di un suolo del modello CRITERIA.
Fig. 1 - Soil water balance scheme of the Criteria model.

proccio dinamico). Mediante l'inserimento di opportuni valori di turno irriguo e di volume di adacquamento è possibile simulare differenti tipologie di metodi irrigui (ad esempio microirrigazione giornaliera o aspersione decadale). Il valore di sensibilità della pianta allo stress idrico indica la percentuale di acqua facilmente disponibile (tra punto di appassimento permanente e capacità di campo) sotto il quale la pianta comincia a risentire dello stesso. Infine, attraverso la percentuale di stress controllato è possibile richiedere al modello di portare la pianta al di sotto della soglia di stress sino ad un ulteriore valore fisiologicamente sopportabile.
In definitiva, l'algoritmo irriguo si può sintetizzare come segue: Criteria controlla se la simulazione si trova all'interno della stagione irrigua, se dall'ultima irrigazione è passato un numero di giorni pari almeno al turno irriguo e se l'acqua facilmente disponibile nello strato radicato (pesata sulla base della densità radicale nei diversi strati di suolo) è inferiore al valore di sensibilità allo stress idrico della coltura. Se tutto ciò si verifica, la coltura potrebbe richiedere irrigazione; viene quindi effettuato un controllo sul rapporto tra traspirazione reale e potenziale avvenuta il giorno precedente. Se il rapporto tra le due è inferiore alla percentuale di stress controllato che l'utente considera accettabile (ad esempio 80%), scatta un'irrigazione pari al volume minimo tra il volume di adacquamento massimo e la quantità di acqua necessaria per riportare alla capacità di campo lo strato radicato (questo per evitare irrigazioni eccessive che si tramuterebbero in perdite da ruscellamento). Il volume irriguo si considera interamente infiltrato nello strato radicato, simulando quindi una irrigazione senza perdite.

LE PREVISIONI STAGIONALI E LA LORO APPLICAZIONE

In Emilia-Romagna, Arpa-Simc produce operativamente previsioni stagionali dal 2007. Per ora i prodotti più affidabili si riferiscono a indici climatici mediati su tre mesi consecutivi. Ciò è dovuto al fatto che su queste scale temporali vi è persistenza di anomalie di temperatura alla superficie del mare nelle regioni tropicali, che rappresentano il "motore" principale del clima e della sua variabilità. Dalle previsioni stagionali si ottengono poi serie sintetiche generate mediante un *weather generator* (Tomei *et al.*, 2009) il cui obiettivo è quello di generare dati climatici giornalieri di temperatura minima e massima e di precipitazione a partire dai valori climatici mensili di sette variabili in ingresso (media della temperatura massima, media della temperatura minima, deviazione standard della temperatura massima, deviazione standard della temperatura minima, media delle precipitazioni totali, frazione di giorni piovosi, scarto tra le temperature massime dei giorni piovosi e asciutti).
Tale *weather generator* viene alimentato con i dati climatici della zona di riferimento e con le previsioni stagionali operative globali di tipo *multi-*

model ensemble EuroSip prodotte presso il Centro Europeo ECMWF (Stockdale *et al.*, 2000) e opportunamente calibrate e regionalizzate, usando la versione MOS dello schema di calibrazione e regionalizzazione (Pavan *et al.*, 2005) (ECMWF Special Project SPIT-SPIA). Ogni serie meteo è quindi composta dai dati meteo locali osservati sino al giorno della previsione e da un trimestre generato. Le previsioni stagionali sopra descritte prodotte per il trimestre estivo giugno-luglio-agosto e i dati regionali dell'uso del suolo rilevati da satellite hanno permesso di sviluppare all'interno del progetto Colt (Classificazione delle colture in atto tramite telerilevamento) uno strumento di individuazione su base geografica delle colture e di valutazione dei consumi idrici attesi tramite il modello Criteria.

L'obiettivo principale del progetto è il monitoraggio a livello regionale dell'uso reale del suolo agricolo su scala annuale per la gestione dell'acqua irrigua. Il risultato della classificazione dell'uso del suolo agricolo e la proiezione di bilancio idrico per il trimestre estivo viene fornito entro fine giugno, in modo da prevedere l'andamento dei consumi idrici durante la stagione estiva.

I principali destinatari del progetto sono i Comprensori di Bonifica regionali e l'area geografica interessata copre la pianura emiliano-romagnola per un totale di circa 1.180.000 ha a prevalente uso agricolo (Fig. 2).

Il progetto si articola in diverse attività; una di queste riguarda la classificazione delle colture agricole in macro gruppi, che avviene tramite l'analisi di serie multitemporali di immagini ottiche da satellite durante il periodo tra novembre 2009 e giugno 2010 da vari satelliti (UK-DMC, UK-DMC2, NIGERIASAT-1). Le finestre di acquisizione (novembre 2009, febbraio, aprile, giugno e luglio 2010) sono state definite in base alle fasi fenologiche individuate nel giardino fenologico gestito dal DISTA dell'Università di Bologna.

A livello operativo la classificazione delle colture è suddivisa in cinque macro-classi (colture erbacee estive, erbacee autunno-vernine, erbacee poliennali foraggere, frutteti e vite, riso) (Tab. 1).

Vengono eseguiti numerosi rilievi in campagna

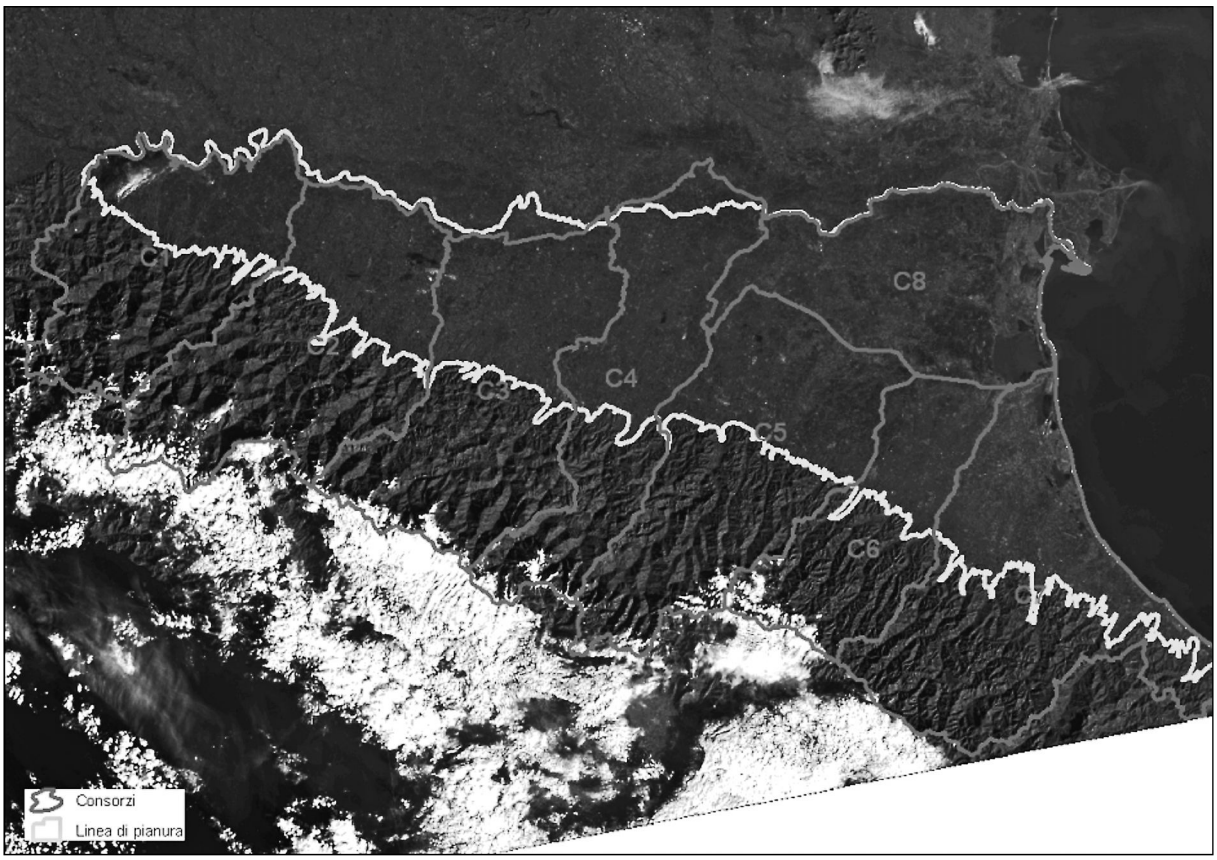

Fig. 2 - Area interessata dal progetto COLT 2010 vista dal satellite.
Fig. 2 - View of the COLT 2010 project study area from satellite.

Macroclasse	Superficie (Ha)	Superficie (%)
Erbacee estive	283.000	36.14
Erbacee autunno-vernine	220.000	28.09
Erbacee poliennali	126.000	16.09
Frutteti e vigneti	108.000	13.79
Riso	5.700	0.73
Aree agricole non classificate (nubi incluse)	40.400	5.16
Totale	**783.100**	**100.00**

Tab. 1 - Distribuzione delle colture nel 2010 distinte per macroclasse. *Tab. 1 - Crop distribution in 2010 divided in macro class.*

allo scopo di raccogliere le verità a terra necessarie alla validazione della classificazione delle immagini. In totale sono stati visitati circa 600 appezzamenti.
Successivamente si procede all'esportazione della classificazione delle colture in atto in un apposito file vettoriale necessario per alimentare il modello del bilancio idrico territoriale, Criteria Geo.
Per ogni consorzio di bonifica sono state poi eseguite le simulazioni con Criteria Geo per il decennio 2000-2009, al fine di ottenere un riferimento climatico, e per il 2010, anno oggetto di studio. Per il primo periodo sono stati utilizzati dati meteorologici osservati provenienti dalla rete Gias mentre per il 2010 sono state utilizzate le previsioni stagionali sopra descritte costituite da più ripetizioni, in modo da avere un discreto campione sul quale poter calcolare i valori medi di irrigazione.
Per quanto riguarda i dati pedologici è stata utilizzata la Carta dei Suoli della Regione Emilia-Romagna.
Per ogni consorzio si è proceduto al calcolo dei fabbisogni irrigui medi per macro-classi di colture e per i mesi di giugno, luglio e agosto dei due periodi (2000-2009 e 2010). I valori medi ottenuti sono stati successivamente cumulati per fornire un'indicazione complessiva sull'intero trimestre. Infine, si è proceduto al confronto tra i fabbisogni irrigui medi dei tre mesi estivi del decennio 2000-2009 con quelli degli stessi mesi del 2010 e alla verifica finale con i dati meteorologici osservati del 2010.

L'UTILIZZO DELLE PROIEZIONI DI CAMBIAMENTO CLIMATICO

L'elaborazione di scenari di cambiamento climatico a medio periodo (2021-2050) si è svolta all'interno del progetto nazionale AgroScenari (Scenari di adattamento dell'Agricoltura italiana ai cambiamenti climatici) per il quale sono state prodotte proiezioni di cambiamento climatico per sei aree italiane (Val Padana, Faentino, Marche, Beneventano, Destra Sele e Oristano) (Fig. 3).

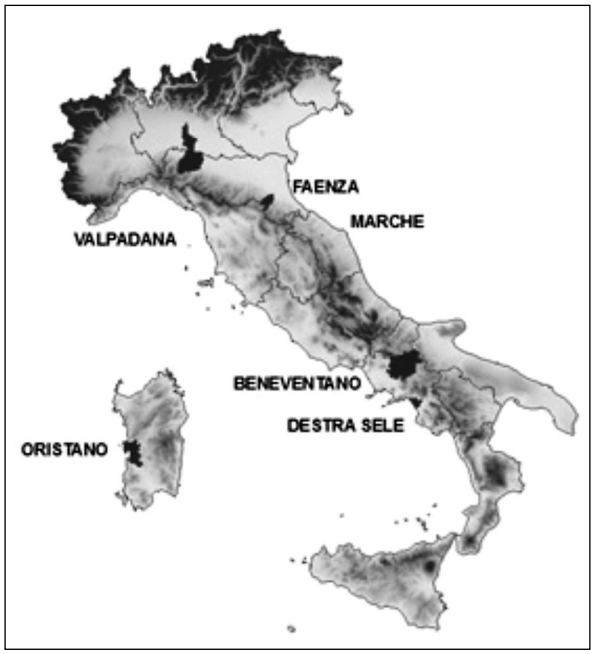

Fig. 3 - Le sei aree di studio del progetto AgroScenari. *Fig. 3 - The six study areas of the AgroScenari project.*

I dati meteorologici utilizzati come riferimento climatico per il trentennio 1961-1990, da cui si è partiti per la produzione di scenari di cambiamento climatico, sono stati estratti dal database delle analisi Ucea.
La regionalizzazione degli scenari è stata ottenuta con tecniche statistiche (Tomozeiu *et al.*, 2007) applicate alle proiezioni di alcuni modelli climatici accoppiati oceano-atmosfera (AOGCM), con scenario di emissione A1B, le cui uscite sono disponibili grazie al progetto europeo Ensembles (Van der Linden e Mitchell, 2009). Il risultato dell'elaborazione finale è costituito da un insieme di serie meteorologiche giornaliere sintetiche, che vengono poi utilizzate come input dal modello Criteria, prodotte mediante il *weather generator* sopra descritto (Tomei *et al.*, 2009), alimentato dalle analisi Ucea e dagli scenari di cambiamento climatico.
Tali serie sintetiche, nell'ambito della linea di ri-

cerca "Irrigazione e cambiamenti climatici" di AgroScenari, sono state utilizzate al fine di valutare l'impatto dei cambiamenti climatici in atto e futuri sui fabbisogni irrigui di colture caratteristiche dell'agricoltura regionale.
Per le analisi del cambiamento climatico in Emilia-Romagna sono stati analizzati i dati appartenenti alle celle della griglia Ucea 1410 (area di Piacenza) e 1362 (area di Faenza), aree caratterizzate rispettivamente da colture orticole come il pomodoro da industria, e da colture frutticole di pregio come il kiwi.
Gli impatti del cambiamento climatico per il periodo 2021-2050 sui fabbisogni irrigui delle colture sono stati analizzati mediante Criteria, nelle due versioni disponibili. L'analisi è stata effettuata a differenti livelli di dettaglio (casi di studio puntuali e territoriali) e sono stati svolti i necessari confronti con le condizioni irrigue a clima attuale. Vengono qui presentati i casi di studio territoriali.
La classificazione delle colture tramite telerilevamento dell'area faentina (corrispondente alla Valle del Lamone) e dell'area piacentina (corrispondente al Consorzio di Bonifica C1 utilizzato anche nell'ambito del progetto COLT 2010) e i dati meteo costituiti dalle analisi Ucea e dalle proiezioni di cambiamento climatico per il periodo 2021-2050 sopra descritte sono state utilizzate per la creazione di casi di studio territoriali mediante Criteria Geo.
Per entrambe le aree di studio, le simulazioni con Criteria sono state eseguite per i due intervalli temporali: 1961-1990 utilizzando le analisi Ucea e 2021-2050 con le proiezioni climatiche.
Sono state calcolate le esigenze idriche stimate per i due periodi e i casi di studio così ottenuti sono stati messi a confronto.
Per analizzare i risultati di Criteria Geo è stato sviluppato il modulo software GeoResultAnalyzer che è in grado di caricare tutti i casi creati dal modello, aggregare nello spazio la grandezza selezionata in base al tipo di aggregazione richiesto (ad esempio la somma sulle aree) per un determinato intervallo temporale, e riportare i percentili della distribuzione di tale aggregazione nei diversi intervalli che intercorrono nel periodo di simulazione (ad esempio nei trent'anni del periodo climatico di riferimento). Questo strumento è stato utilizzato per l'analisi delle richieste irrigue delle colture agrarie nei differenti casi di studio analizzati.

Consorzio di Bonifica	Periodo	Irrigazione stimata da previsioni stagionali	Irrigazione 2010 stimata dai dati meteo misurati
C1	Giugno	65.66	32.67
	Luglio	109.54	66.25
	Agosto	123.38	77.55
	Cumulato trimestrale	98.41	57.90
C2	Giugno	35.93	31.50
	Luglio	70.84	103.22
	Agosto	163.62	23.33
	Cumulato trimestrale	76.21	64.79
C3	Giugno	55.38	8.19
	Luglio	92.57	86.43
	Agosto	89.94	14.33
	Cumulato trimestrale	83.92	44.88
C4	Giugno	111.81	14.39
	Luglio	106.16	108.88
	Agosto	179.71	47.29
	Cumulato trimestrale	125.67	73.84
C5	Giugno	61.10	1.06
	Luglio	107.59	86.37
	Agosto	125.89	25.95
	Cumulato trimestrale	98.84	49.71
C6	Giugno	36.01	0.98
	Luglio	88.02	102.43
	Agosto	135.01	24.85
	Cumulato trimestrale	82.20	57.52
C7	Giugno	135.18	4.53
	Luglio	119.72	124.94
	Agosto	182.34	10.61
	Cumulato trimestrale	136.27	72.98
C8	Giugno	89.12	11.65
	Luglio	109.21	58.45
	Agosto	163.61	40.89
	Cumulato trimestrale	120.10	46.81

Tab. 2 - Risultati ottenuti nel progetto COLT 2010 nei singoli consorzi di bonifica (% rispetto all'irrigazione media del periodo 2000-2009).
Tab. 2 - Results obtained in the project COLT 2010 for the Reclamation Consortia (% with respect to the mean irrigation referred to the period 2000-2009).

RISULTATI

Analizzando i risultati cumulati trimestrali di ogni singolo consorzio di bonifica (Tab. 2) è possibile constatare che in tre casi (consorzi C2, C3, C6) è stata correttamente prevista la diminuzione delle necessità irrigue rispetto all'irrigazione media del periodo 2000-2009, in due casi (C1, C5) è stata prevista una sostanziale stabilità, mentre negli ultimi tre casi (C4, C7, C8), a fronte della previsione di maggiori esigenze irrigue, è stata riscontrata un'effettiva diminuzione.

Dall'analisi dei dati derivati dall'applicazione delle proiezioni di cambiamento climatico, per il piacentino sono state messe a confronto le esigenze irrigue delle colture dell'areale per i periodi 1961-1990 e la proiezione 2021-2050. Dal confronto è emerso un marcato aumento della richiesta irrigua per il periodo 2021-2050 rispetto al trentennio 1961-1990. Analizzando la distribuzione dei volumi irrigui medi annui nei due periodi (Fig. 4), si può notare che la mediana si attesta per il 1961-1990 sui 740 m³/ha mentre per il 2021-2050 essa raggiunge i 780 m³/ha. Inoltre il valore massimo delle distribuzioni per il clima di riferimento è 1107 m³/ha mentre per le proiezioni future esso raggiunge i 1194 m³/ha. Per i valori del 5°, 25°, 75° e 95° percentile si osservano notevoli differenze nei volumi di adacquamento tra i periodi 1961-1990 e 2021-2050 (mediamente +100 m³/ha).

Per il faentino (Fig. 5) si può osservare che le proiezioni future mostrano un leggero aumento dei fabbisogni irrigui. Le mediane per entrambi i periodi si attestano sullo stesso valore (circa 980 m³/ha); il 5°, il 75° e il 95° percentile risultano maggiori per il periodo 2021-2050, mentre per il valore minimo, il valore massimo e il 1° percentile il periodo 1961-1990 presenta necessità irrigue leggermente maggiori.

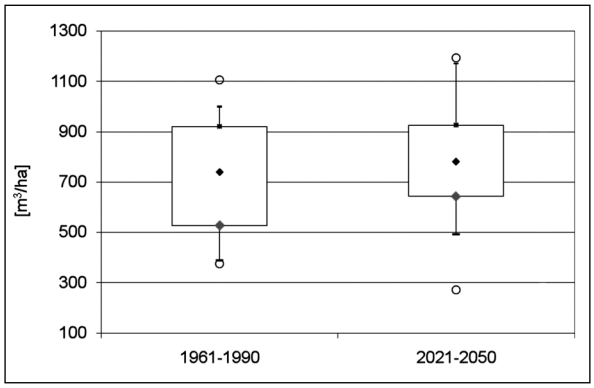

Fig. 4 - Confronto delle distribuzioni dei fabbisogni irrigui medi della totalità delle colture stimati per il piacentino per gli scenari 1961-1990 e 2021-2050.

Fig. 4 - Distribution comparison of the simulated mean irrigation water needs for all the crops in the Piacenza area for the periods 1961-1990 and the climate change scenario 2021-2050.

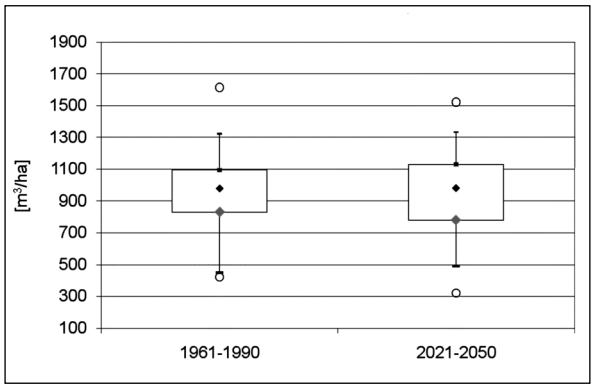

Fig. 5 - Confronto delle distribuzioni dei fabbisogni irrigui medi della totalità delle colture stimati per il faentino per gli scenari 1961-1990 e 2021-2050.

Fig. 5 - Distribution comparison of the simulated mean irrigation water needs for all the crops in the Faenza area for the period 1961-1990 and the climate change scenario 2021-2050.

CONCLUSIONI

I risultati ottenuti per il trimestre estivo 2010 con il modello di bilancio idrico Criteria insieme alle previsioni stagionali sono coerenti con il bilancio idrico calcolato a posteriori con i dati meteo osservati, ciò significa che il modello, se opportunamente calibrato e validato, potrebbe essere utilmente impiegato anche in areali di coltivazione differenti da quelli della pianura emiliano-romagnola.

L'applicazione delle proiezioni di cambiamento climatico per il trentennio 2021-2050, mostra che non è previsto un sensibile aumento delle esigenze irrigue delle colture: ciò è giustificato dal fatto che l'incremento della temperatura (+2 °C) e la diminuzione delle precipitazioni estive (-20%) previsti dai modelli, sono compensati dal previsto aumento delle precipitazioni primaverili (+25%).

I risultati ottenuti sono un esempio dell'utilizzo di Criteria nel contesto climatico, agronomico e pedologico delle aree di pianura della regione Emilia-Romagna. Il modello rappresenta, pertanto, uno strumento utile per la gestione delle risorse irrigue e ciò è particolarmente importante alla luce dei cambiamenti climatici in atto e futuri.

RINGRAZIAMENTI

Questo articolo prende avvio dalla tesi di Master dal titolo "La gestione delle emergenze idriche indotte da siccità e scenari di adattamento dell'agricoltura ai cambiamenti climatici in Emilia-Romagna" che

è stata discussa dal Dr. Andrea Gallo per l'Anno Accademico 2009/2010 all'interno del Master di II livello in "Gestione del rischio indotto da disastri naturali". Si ringraziano il relatore e il correlatore della tesi, Prof. Alberto Lamberti e Prof. Alberto Montanari.
Il progetto AgroScenari è realizzato su finanziamento CRA-Mipaaf (www.agroscenari.it). The Ensembles data used in this work was funded by the EU FP6 IP Ensembles (Contract nr 505539) whose support is gratefully acknowledged.

BIBLIOGRAFIA

IPCC, 2007. *Climate Change 2007: Synthesis Report. Contribution of Working Groups I, II and III to the Fourth Assessment Report of the Intergovernmental Panel on Climate Change*. Core Writing Team, Pachauri R.K and Reisinger A. (eds.). IPCC, Geneva, Switzerland, 104 pp.

Marletto V., Ventura F., Fontana G., Tomei F., 2007. *Wheat growth simulation and yield prediction with seasonal forecasts and a numerical model*. Agricultural and forest meteorology, 147: 71-79.

Marletto V., Antolini A., Tomei F., Pavan V., Tomozeiu R., 2010. *Atlante idroclimatico dell'Emilia-Romagna 1961-2008*. Quaderni di ARPA, ISBN 88-87854-24-6.

Pavan V., Marchesi S., Morgillo A., Cacciamani C. and Reyes F.D., 2005. *Downscaling of DEMETER winter seasonal hindcasts over Northern Italy*. Tellus, 57A: 424-434.

Ragab R., Prudhomme C., 2002. *Climate Change and Water Resources Management in Arid and Semi-arid Regions: Prospective and Challenges for the 21st Century*. Biosystems Engineering, 81 (1): 3-34.

Stockdale T., Doblas Reyes F.J., Ferranti L., 2000. *EUROSIP: multi-model seasonal forecasting*. ECMWF Newsletter No. 118.

Tomei F., Villani G., Pavan V., Pratizzoli W., Marletto V., 2009. *Report on the quality of seasonal predictions of wheat yield and irrigation needs in Northern Italy*. Ensembles Project, 6th Eu R&D Framework Programme, Research Theme 6, Assessments of Impacts and Climate Change, available as Deliverable 6.22 from www.ensembles-eu.org

Tomozeiu R., Cacciamani C., Pavan V., Morgillo A., Busuioc A., 2007. *Climate change scenarios for surface temperature in Emilia-Romagna (Italy) obtained using statistical downscaling models*. Theoretical and Applied Climatology, 90: 25-47.

Van der Linden P., Mitchell J.F.B., 2009. *ENSEMBLES: Climate Change and its impacts: Summary of research and results from the ENSEMBLES project*, Met Office Hadley Centre, UK, 160 pp.

High-resolution hail monitoring in an alpine fruit-growing region

Emanuele Eccel[1*], *Fabio Zottele*[2]

Abstract: *The hail monitoring network in Trentino has been uninterruptedly run since 1974. It consists of 271 impactometric measurement sites, arranged according to a 2-km regular grid. Recorded data allow an estimation of the kinetic energy of the hailstorm. To investigate the acknowledged correlation between electric activity of thunderstorm cells and the amount of hail fallen during hail, in this study consideration is given to two aspects: i) the relationship between ground lightning measures and hail indices; ii) some spatial and altitudinal features of hail climatology. Hail data were aggregated in one hail season per year, from May to September. The correlation of hail indices with elevation is clear, yet it cannot fully explain the inhomogeneous distribution in some areas, where local features significantly affect hail occurrence. The statistical link between annual hail values and the total measured number of lightning flashes is also good; for some indices it is highly significant ($p<0.01$) after the removal of respective time trends. This allows to propose the use of the number of lightning flashes over a hail season as a good indicator of hail fallen in the same period.*
Keywords: *hailstorms, Trentino, lightning, spatial interpolation.*

Riassunto: *La rete di monitoraggio grandine in Trentino è operativa continuativamente dal 1974. Essa consiste in 271 siti di rilievo impattometrici disposti secondo una griglia di lato approssimativo 2 km. Il rilievo consente di stimare l'energia cinetica della grandinata. Per investigare la nota correlazione tra l'attività elettrica delle celle temporalesche e la quantità di grandine caduta durante gli eventi grandigeni, in questo studio sono esaminati due aspetti: i) la relazione tra misure di fulmini al suolo e gli indici di grandine; ii) alcune caratteristiche spaziali ed altitudinali della climatologia della grandine. I dati di grandine sono stati aggregati su base annuale (in un'unica stagione, da maggio a settembre). La correlazione degli indici di grandine con la quota è chiara; essa però non può spiegare da sola la distribuzione non omogenea in alcune aree, dove effetti locali influenzano significativamente l'occorrenza della grandine. Anche la relazione trovata tra i valori annuali di grandine e il totale di fulmini rilevati è buona per la maggior parte degli indici, per alcuni di essi altamente significativa ($p<0.01$) dopo aver rimosso i rispettivi trend temporali. Ciò consente di proporre la misura dei fulmini registrati, a livello stagionale, come un buon indicatore della grandine caduta nella medesima stagione.*
Parole chiave: *grandinate, Trentino, fulmini, spazializzazione.*

1. INTRODUCTION

There is a general agreement on the observed increase in climatic extremes, like floods, heat waves and hailstorms in the last decades, in Europe as well as in other regions of the world (Munich Re., 1999; Brunetti *et al.*, 2002; Coleman, 2003; Meehl *et al.*, 2007). This is one likely consequence of the ongoing climate change, although a major role may have been played by an increase in vulnerability in the demographic and urban settlement structure in many parts of the world. In the Alpine area storms, among the meteorological adversities encompassing all kinds of intense activity connected to severe weather conditions, represent the second major cause of economic damages and the first cause of insured damages related to natural hazards. Hail is responsible for extreme, though localized, damages, becoming an outstanding source of economic loss even for goods other than crops. Historical hailstorms highlight the relevant potential risk in Europe; in 1984 an ominous event in Munich, Germany, caused around 1.5 billion € damage, of which about 750 million € was insured (SwissRe, 2006).

In Italy, the northern regions are particularly affected by hail (Berz and Siebert, 2000). In the Alpine region of Trentino, hail alone represents by far the most important meteorological adversity to its valuable crop production. The harm is not only due to the loss of the harvest itself, in case of very severe events, but also to the economical depreciation of the crop, when the damage is not so severe to destroy the harvest. In this region, agricultural damages, almost entirely referred to apple and grapevine, ranged, in the

* Corresponding Author: emanuele.eccel@ismaa.it
[1] Sustainable Agro-ecosystems and Bioresources Department, IASMA Research and Innovation Centre, Fondazione Edmund Mach
[2] Centre for Technology Transfer, Fondazione Edmund Mach San Michele all'Adige, (TN), Italy
Received 27 October 2011, accepted 21 February 2012.

period 2003 – 2008, from 3.6% (2004) to 16.6% (2008) of the insured capital, with an average of 10.0% (A. Berti, pers. comm.). An analysis of the hail climatology by Eccel *et al.* (2012) for Trentino shows that in the last decades this phenomenon has remained mostly unchanged in its average features (like the number of episodes or the hit surface), whereas its more extreme aspects have undergone a remarkable increase.

Hail measurement is a time-consuming activity. The simple recording of the hail event in terms of "present weather" – currently done by all the Global Telecommunication System (GTS) stations around the world – results in too coarse a resolution for a proper sampling of the effects of deep-convection. Due to its large variability in space, its short duration (minutes to a score of minutes) and the extremely local scale of the phenomenon ("hail streaks" have dimensions of a few km by a few hundreds of meters), a thorough hail monitoring over a territory requires a high-resolution network, typically made up of hundreds of hailpads. Hence, dense hail networks in the Alpine region (not differently from other areas in the world) are scarce and they are far from covering all the potentially affected territory. Even when they exist, their coverage focuses in general on the most sensitive areas, namely cropland, neglecting the others. For example, networks are operated in the Alpine regions of Styria, Trentino, Friuli and Slovenia, as well as in Spain and in France, just to mention European countries.

The increasing use of advanced radar techniques (particularly, the dual polarisation facilities allow the identification of hail in cumulonimbus cells – Sugier and Tabary, 2006), the development of hailpad networks has apparently eased off, owing to complexity and cost issues for its maintenance, and interest in hail measurement has turned to alternative methods. Probably also because of such restrictions, the number of climate studies based on impactometric data is relatively small (Dessens and Fraile, 1994; Sànchez *et al.*, 1996; Eccel and Ferrari, 1997; Vinet, 2001; Fraile *et al.*, 2003; Giaiotti *et al.*, 2003, Berthet *et al.*, 2010; Eccel *et al.*, 2012; Manzato, 2012).

This is not the place to review the state of the art of the investigation on radar skill in hail detection and measurement; the datasets created by this technique have, of course, an extremely high resolution in both time and space, but also large inhomogeneities. Another easily measurable physical quantity of thunderstorm cells is their electric activity. There have been a number of studies on this subject, mostly focussing on the physics of the phenomena (like one very recent from Emersic *et al.*, 2011), generally investigating the relationships between lightning and hail at the atmospheric cell level. In the USA, Changnon (1992) reported that lightning activity is strongly associated with hail occurrence, even if the areas of most severe hail damage do not coincide with those of most intense flash records. In Switzerland, Hohl and Schiesser (2001) found an excellent relation (r=0.95) of hail kinetic energy with negative cloud-to-ground lightning flashes (the majority of them), but not for the positive ones, and suggest the use of this indicator as nowcasting predictor for intense hailstorms. The same scale of investigation (cloud cell) yielded different results in southern France (Soula *et al.*, 2004): the highest number of lightning flashes was associated to no-hail-bearing thunderstorms, even if the authors state that often positive flashes were observed in such cases, depressing their negative proportion.

Far from trying to add a contribution to the physical comprehension of the phenomenon, the present work aims at checking a very simple technique - cloud-to-ground lightning survey - for thunderstorm detection. The statistical correlation with hail activity makes it suitable for climate purposes, rather than for operational nowcasting applications. The discussion is enriched by the analysis of some spatial interpolation of basic hail quantities, allowed by the high-resolution quantitative measurements from the local hailpad network.

2. STUDY AREA, DATA, AND METHODOLOGY

The geographic and climatic context

Trentino (central-eastern Italian Alps – Fig. 1) is a system of major valleys, among which the longest is 'Val d'Adige'. The cropland is mostly devoted to apple and grapevine growing. In general, climate in Trentino can be ascribed to the humid, temperate, oceanic type, particularly in the pre-alpine areas, more open towards the Po Plain and the Adriatic See. Some areas show features of transition to a more continental-alpine climate, cooler and often drier, more typical of the inner mountain valleys. Albeit precipitation amounts are mostly distributed over two maxima (autumn and spring), in some mountain areas rainfall peaks in summer (Eccel and Saibanti, 2007). The higher and inner areas receive an important supply of rainfall from summer thunderstorms, thanks to orography-induced mechanisms of convective instability triggering. For this reason, like in many other

Fig. 1 - The study area (Trentino, Italy). The contour of the province is in bold.
Fig. 1 - L'area di studio (Trentino). Il contorno della provincia è in grassetto.

regions of the Alps, hailstorms are more frequent and more intense in elevated areas.

The hail monitoring network

The measurements are performed by "Schleusener"-type, 15 cm x 15 cm polystyrene hailpads, covered with a 0.135 mm thick aluminium sheet (Schleusener and Jennings, 1960). The pad is mounted horizontally on a bearing fixed at 1 m from the ground. Each hailstone leaves a dent on the aluminium sheet, whose depth (and hence its horizontal dimension) is proportional to its kinetic energy. After inking, the dents are counted and measured.

The hail monitoring network in Trentino, established in 1974 and since then continuously operated, covers the main agricultural areas, with roughly square grids of 2 km's side, as regular as possible. It ranges from an elevation of 70 m to 1260 m a.s.l., with 271 sites altogether (Fig. 2 – the mapped hail indices are discussed in section 3). The cropland is mostly devoted to apple and grapevine growing. Only minor changes in the network (expiry of sites and addition of new ones) occurred over the years. The measurement season starts on 1st May and ends on 30th September, only exceptionally

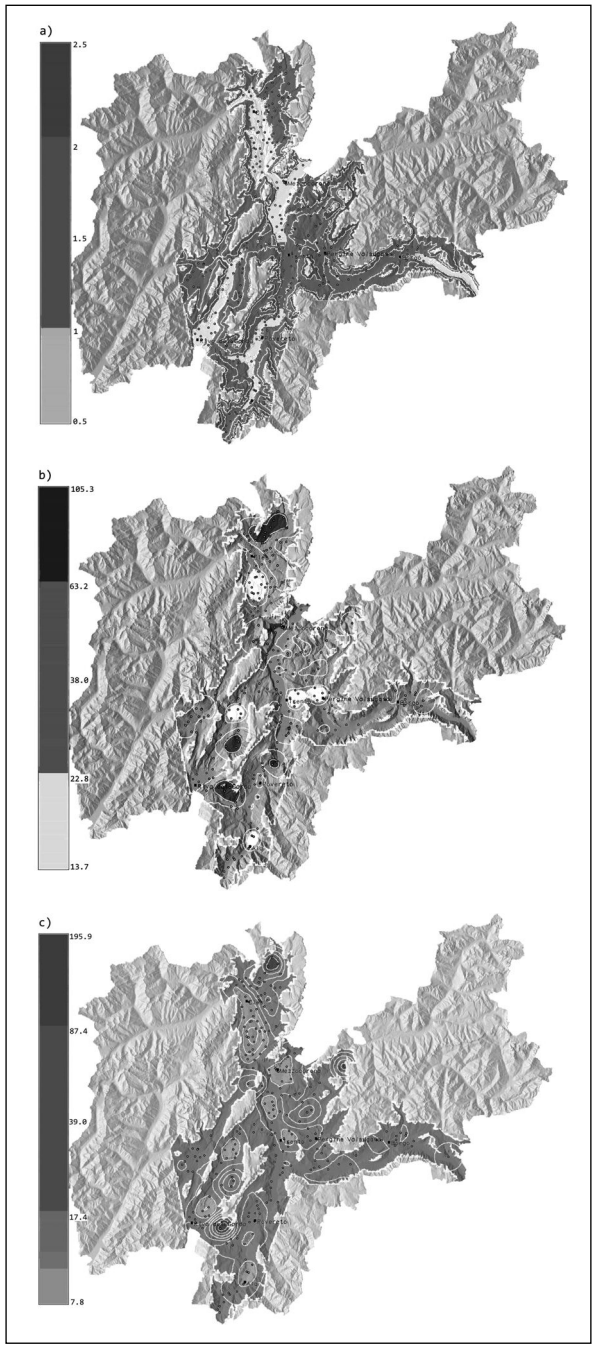

Fig. 2 - Map of Trentino orography with spatial interpolation of three hail indices. a) mean nr. of hail occurrences per hailpad. b) kinetic energy, average over all reports (m.en_rep, see Appendix) (J m^{-2} - log scale). c) mean annual cumulated kinetic energy (m_tot_en, see Appendix) (J m^{-2} - log scale). Spatial interpolation carried out with kriging with external drift (height), 40-m resolution.
Fig. 2 - Mappa del Trentino con la spazializzazione di tre indici di grandine: a) numero medio di occorrenze di grandine per grelimetro. b) energia cinetica media (J m^{-2} – scala logaritmica). c) media annua dell'energia cinetica cumulata (J m^{-2} – scala logaritmica). Spazializzazione realizzata con kriging con forzante esterna (altitudine), risoluzione 40 m.

earlier or later, if important events occur before or after this standard season.
Data are gathered after each hailstorm. Each hailpad reading yields one hail "report", which is the survey unit of the hail network. One "event" is made up from all the reports recorded on the same date. Of course, there are a few cases of events occurring around midnight that are ascribed to two different days, according to the time of occurrence. The opposite case is when two separate events occur at different times in the same day, and are counted as one. Given the small number of cases, and considering that the first case (overestimation of events) acts in the opposite way of the second (underestimation of events), the error was neglected, also because in this work hail data were aggregated over the seasons.
Volunteer observers substitute each hailpad after it is impacted and fill in a report with ancillary information on the hailstorm. Hailpads are sent to the agency that operates the network (GIS Unit of E. Mach Foundation – FEM - http://meteo.iasma.it/meteo/), where they are inked and interpreted (hailpad reading protocol and calibration in Montefinale *et al.*, 1982). Each dent is assigned to one diameter class (there are seven), each identifying a specific kinetic energy. The total energy comes from the product of the number of hailstones in each class by the specific kinetic energy for the class itself.
Only the vertical component of kinetic energy was considered. From dent counting and measurement, given the proportionality of both hailstone diameter (d) and its terminal velocity to the dent, the kinetic energy Ek of each hailstone is (details in Eccel *et al.*, 2012)

$$Ek \propto d^4$$

Lightning measurements
As lightning is an indicator of thunderstorm, its measurement was used to compare hail indicators to the total thunderstorm activity in the period 1996-2009. Lightning flashes were retrieved from the Italian lightning monitoring network (CESI – SIRF: http://sirf.cesi.it). The network is formed by 16 sensors positioned on the Italian territory. Ten more sensors are used as well, located beyond the Italian border, to enhance the network sensitivity. Each sensor is connected by a dedicated line to CESI's operational centre in Milan.
All the sensors use IMPACT technology (Global Atmospherics Inc.), and make use of broadband electromagnetic antennas, with GPS synchronization, Time Of Arrival (TOA) and Magnetic Direction Finding (MDF) calculation methods. They detect the electromagnetic field emitted by each cloud-ground lightning, providing raw data (electromagnetic field vector, time, etc.). Each sensor is able to discriminate a lightning signal from the background noise. Being the electro-magnetic field disturbance very quickly and clearly detected by the network, the time resolution is very high (fractions of second). The space resolution allows to locate the falling site of a lightning stroke in the range of about 500 m from the exact point. In general, both time and space resolution of the SIRF (Sistema Italiano Rilevamento Fulmini) network are higher than the corresponding resolutions of the hail network.
The data were aggregated over the territory of Trentino by CESI-SIRF and summed yearly for the period May – September, the same as for the hail monitoring. Both the whole administrative region (province of Trento) and the area restricted to the impactometric network domain were considered for the spatial aggregation of lightning data.

Data processing
Measuring and collecting hail data with the detail of each single class of hailstone diameter provide a huge amount of information. In this work, data processing for hail climatology was rather trivial: values were processed as single reports (for example, to extract maxima), and reports were aggregated by event (each identified by one single day) and by season (one hail season per year). Extreme values were investigated as both absolute maxima and 90th percentiles. An explanation of all hail indices is given in the Appendix. The analysis of the link of hail indices with the electric activity consisted of the assessment of the correlation between each couple of seasonally-aggregated hail index vs. lightning flash count.
The spatial interpolation of three basic hail indices (nr. of hail days, mean kinetic energy, accumulated kinetic energy) was carried out by kriging with external drift (elevation), implemented in the open-source R code, library "gstat" (R Developing Core Team, 2011) and graphically represented by the open-source GIS GRASS (GRASS Development Team, 2010). The resolution of the spatial interpolation was 40 m. In order to avoid extrapolation of data in non-monitored areas, the analysis was restricted to the area of Trentino that falls within the limits of the hail network and lies below 1200 m a.s.l. (Fig. 2)

3. RESULTS AND DISCUSSION

Correlation with lightning totals
From the visual assessment of the time series of the total number of lightning flashes per year (NLF)

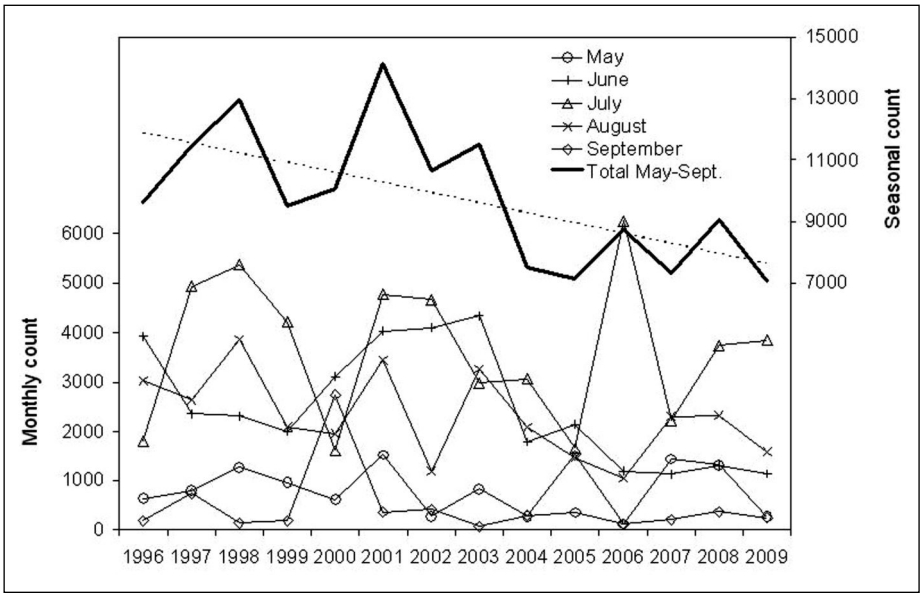

Fig. 3 - Number of lightning strokes (NLS) for the whole Trentino area, in the five months of the hail-monitoring season. Thin lines: monthly counts. Thick line (and dashed linear interpolation line): total seasonal count. Data obtained from CESI-SIRF.
Fig. 3 - Numero di fulmini (NLS) per l'intera area trentina, nei cinque mesi della stagione di monitoraggio grandine. Linee sottili: conteggio mensile. Linea spessa (e linea tratteggiata interpolante): conteggio stagionale totale. Dati rilevati da CESI-SIRF.

over the area covered by the hailpad network in Trentino, there has been a general decrease in the period 1996-2009 (Fig. 3), significant with $p<0.05$. More precisely, it can be seen that every hail season in the series from 2004 to 2009 had lower values than any others in the 1996-2003 period. This trend results from the sum of single months: a significantly ($p<0.05$) decrease can be found for the month of June, but not for the other months. Similar results were obtained when considering the whole region (Trentino).
The correlation between hail indices and NLF can be calculated using both raw or time-detrended series to discard the effects of independent time trends for both phenomena. The coefficients of determination R^2 are reported in Tab.1 and the scatterplots of the annual series in Fig. 4 and Fig. 5. It could be argued that, while seasonal NLF decreases over the period, many hail indices, namely those that express kinetic energy –especially of intense episodes - are increasing (Eccel *et al.*, 2012), suggesting an opposite time trend for hail in the same observational period. Because the two phenomena are aspects of the same atmospheric

Hail index	whole region		hail network area	
	raw	detrended	raw	detrended
cum_hit_surf_dens	NS	0.362	0.305	0.384
hail_days	NS	NS	NS	NS
m_surf_ev	0.349	0.349	0.287	NS
cum_en_dens	NS	**0.454**	NS	0.339
m.en_rep	NS	0.349	NS	NS
sd_en	NS	0.372	NS	NS
m_ev_en	NS	NS	NS	NS
m_tot_en	0.288	**0.490**	NS	NS
max_en_rep	NS	0.405	NS	NS
extr_en_rep	NS	0.303	NS	NS
tot_en_max_ev	0.363	**0.475**	NS	NS
tot_en_extr_ev	NS	0.303	NS	NS

Tab. 1 - Coefficients of determination R2 of hail indices and total number of cloud–to-ground lightning flashes (NLF) over whole Trentino region and over the impactometric network area. Only figures with $p<0.05$ are reported. In bold if $p<0.01$. NS: non-significant. See Appendix for acronyms.
Tab. 1 - Coefficienti di determinazione R2 tra indici di grandine e numero totale di fulmini nube – suolo (NLF) sull'intero territorio trentino e sulla sola area coperta dalla rete impattometrica. Sono riportati solo i casi con $p<0.05$. In grassetto se $p<0.01$. NS: non significativo. Consultare "Appendix" per i dettagli sugli acronimi.

agent – the cumulonimbus activity –a negative link between them is hardly explainable. For this reason, to discard the effects of independent mechanisms that lead to either decrease or increase of single variables, the pairs of hail indices – NLF were detrended, to isolate and highlight the statistical relationship.

Indeed, there is a general increase in the correlation (and significance) between hail indices and NLF after detrending, with some pairs significant at $p<0.01$ (panels b), f), and i) in Fig. 4); the latter represent: accumulated energy density (cum_en_dens), mean total energy (m_tot_en), and total kinetic energy for the maximum annual event (tot_en_max_ev). While the link between total amount of lightning in a hail season and the corresponding accumulated hail measures is quite natural, it is interesting to comment the high statistical link between the most severe seasonal event(s) (also the 90th quantile event – tot_en_extr_ev, Fig. 4d - shows a significant statistical link with NLF) and total season lightning. This result is a consequence of the strong link between the most severe event and the total kinetic energy accumulated over the whole season: the most important event is on average responsible for – roughly – the half of the total kinetic energy of the hail season (Eccel and Ferrari, 1997). The number of events (hail_days, Fig. 4e), and consequently their mean energy (m.en_rep), are poorly "explained" by the NLF alone, if this is considered a "predictor". None of these two

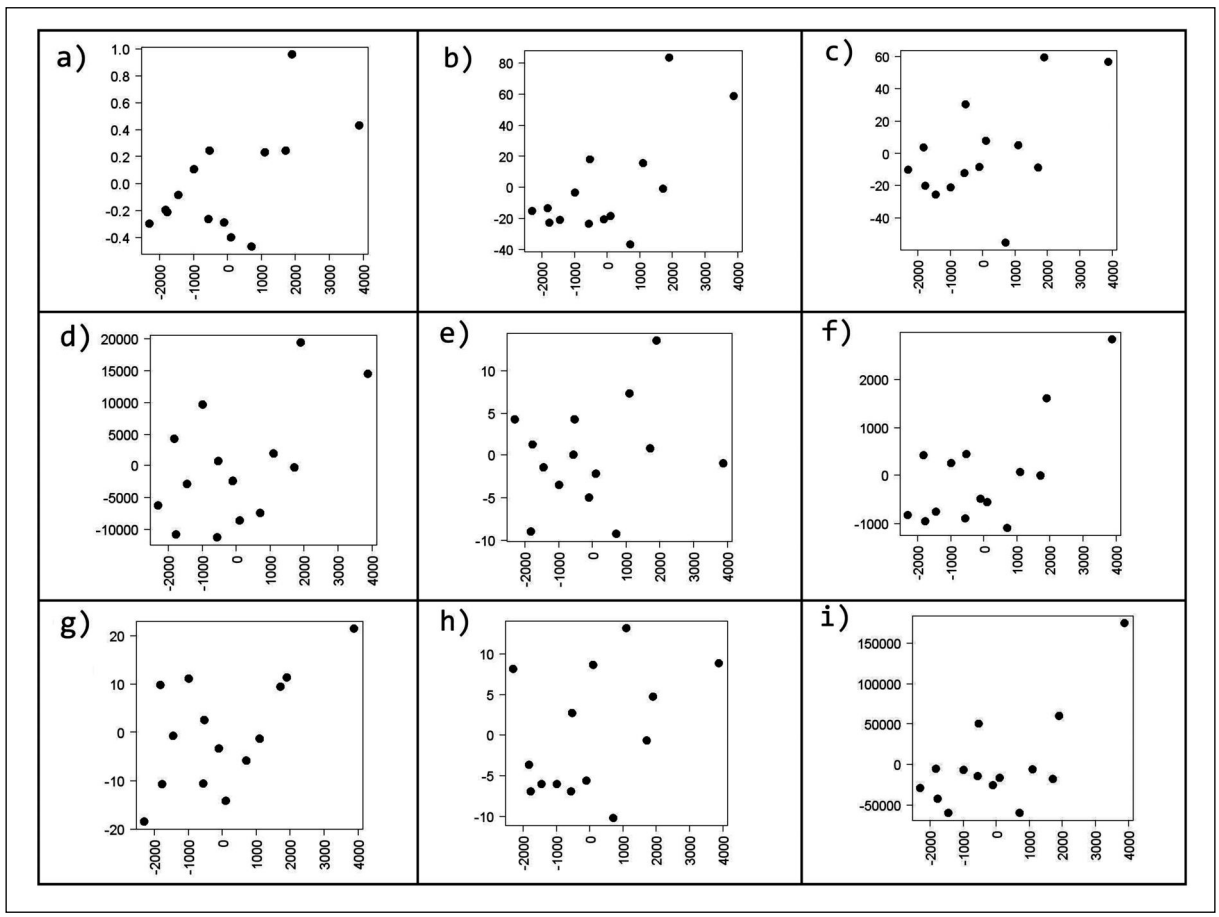

Fig. 4 - Detrended scatterplots of anomalies of hail indices vs. NLS (seasonal number of strokes) over Trentino. Period: 1996-2009. a) cum_hit_surf_dens b) cum_en_dens c) extr_en_rep d) extr_tot_en_ev e) hail_days f) m_tot_en g) m_surf_ev h) m_ev_en i) tot_en_max_ev (see Appendix for key). See also Tab.1 for numeric values of the coefficients of determination and their significance.

Fig. 4 - Grafici a dispersione delle serie detrendizzate delle anomalie degli indici di grandine vs. NLS (numero stagionale di fulmini) sul Trentino. Periodo: 1996-2009. a) cum_hit_surf_dens b) cum_en_dens c) extr_en_rep d) extr_tot_en_ev e) hail_days f) m_tot_en g) m_surf_ev h) m_ev_en i) tot_en_max_ev (consultare "Appendix" per il significato). Vedere anche la Tab.1 per i valori numerici dei coefficienti di determinazione e la loro significatività.

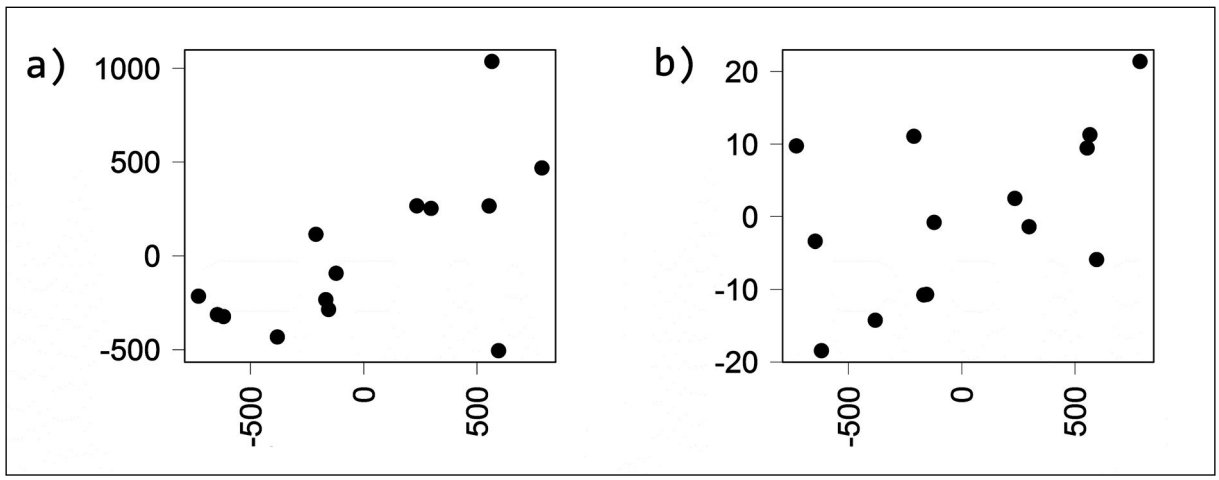

Fig. 5 - Scatterplot of detrended anomalies of hail indices vs. NLF (seasonal number of cloud–to-ground lightning flashes) over the area covered by the impactometric network in Trentino. Period: 1996-2009. a) cum_hit_surf_dens. b) cum_en_dens (see Appendix for key). See also Tab.1 for numeric values of the coefficients of determination and their significance.
Fig. 5 - Grafici a dispersione delle serie detrendizzate delle anomalie degli indici di grandine vs. NLF (numero stagionale di fulmini nube - suolo) sull'area coperta dalla rete impattometrica trentina. Periodo: 1996-2009. a) cum_hit_surf_dens b) cum_en_dens (consultare "Appendix" per il significato). Vedere anche la Tab.1 per i valori numerici dei coefficienti di determinazione e la loro significatività.

indices refer directly to the total kinetic energy for season, which is the most important index, being strongly correlated to the real hail damage to crops and goods.
The coefficients (not shown) are always positive: the more lightning, the more hail. Indeed, if one considers the period 1996-2009, there is no hail index that shows a significant time trend at $p<0.05$; some of them (the mean surface for event, m_surf_ev, or the maximum total energy for event, tot_en_max_ev) display a negative time trend, even if with a very low significance (data not shown).
When the spatial domain of lightning measurement is restricted to the area actually covered by the hail monitoring network, and not to the whole administrative region (province of Trento), the correlation between lightning activity and hail decreases. This issue deserves some attention. In general, in the case of "restricted area", detrending does not increment correlations in such an evident way as it does when the whole region is considered for lightning measurement. However, the two most important hail indices (the accumulated hit surface density, cum_hit_surf_dens, and the total kinetic energy density, cum_en_dens) do show good links with the electric activity in the hail season (table 1).
An explanation for the displacement of hail with respect to lightning would require a thunderstorm-cell-scale analysis. Changnon (1992) reported, for the USA, a general space and time gap between maximum flash rate and hail. There are important differences when dealing with single events. In the same work by Changnon, it is stated that the number of flashes was well related to hail severity, but also that 75% of the lightning centres were not associated with hail. However, in this study, as already stated, the issue has not bee tackled at the event scale. Further comments on the difference in the most frequent locations of lightning and hail are given at the end of next section.
It can be concluded that both lightning and hailstorm activities may show their own time trends, but, when the latter are removed from the series, the correlation between the two phenomena become clearer. This was not an unexpected result, keeping in mind that both lightning and hail are measurable effects of thunderstorm cell activity. The good correlation between some hail indices and lightning activities suggests its use as a proxy for hail incidence in an area, at least from a climatic point of view.

Spatial and altitudinal patterns of hail

Spatial interpolation of hail data (Fig. 2) was restricted to a narrow region that extends from the hail network domain to cover the main agricultural valleys of Trentino. It is a limited area, nevertheless it comprises the majority of the grapevine and apple production farms in the region. This analysis encompassed all data recorded for the period 1974-2008.
With the exception of mean kinetic energy, all indices

(number of events, accumulated kinetic energy, maximum recorded energy) exhibit a significant positive correlation with altitude (Tab. 2). However, interesting geographic patterns appear when the data are reported on the map (Fig. 2). The mean annual number of occurrences at the most hail-prone site is 3.6 times higher than at the less-prone one (Fig. 2a). In general, elevated sites are more prone to hail occurrence, but the relationship is uneven, with the highest frequency occurring in the central-eastern part, not equalled by other mountain areas. More interesting hints come from the analysis of kinetic energy maps (Fig. 2b). Mean energy (per report) shows a polycentric pattern, with single spots exceeding the general average. This index expresses the mean kinetic energy, irrespective of the average number of events occurring at the site. More useful is the map of accumulated kinetic energy (Fig. 2c), which is the index most strongly linked to the crop damage. The spatial pattern is more even: mean energy peaks are smoothed, due to the co-occurrence of a lower number of episodes recorded in such areas. However, even in a relatively small region like the agricultural area of Trentino, there is an evident heterogeneity, not always explainable by altitude only. For example, in the 'Val di Non' there is a clear gradient in hail severity moving from SW to NE, namely from the right to the left of the Noce river valley. The other two "hot spots" (the 'Val di Gresta' and the area between the 'Val di Cembra' and the 'Altipiano di Piné') are both influenced by the presence of single high-elevation hailpad sites (see Fig. 2c).

Another aspect can add insight to the issue of hail displacement with respect to lightning. Fig. 6 shows the total number of lightning flashes in the period 1996-2010 over the area corresponding to the hail network coverage, at the resolution of 1 x 1 km^2. The survey period only partially overlaps with that of Fig. 2, but some features can be recognized from both sources, namely the maximum in the "central" area, south and north of Trento (compare Fig. 6 with Fig. 2b – kinetic energy, m.en_rep). There is no evidence of a general lightning increase with elevation. Even if based on qualitative inference, this observation is consistent with the higher correlation between hail activity and lightning measurement, when the monitoring domain is extended to a larger, regional area.

Hail index	Trend / 100 m height
cum_hit_surf [km^2]	0.4
m_tot_en [J m^{-2}]	8.3
m.en_rep [J m^{-2}]	2.6
max_en_rep (annual mean) [J m^{-2}]	5.7

Tab. 2 - Correlations of hail indices (each referred to single hailpads) with measurement heights (trends expressed over 100 m height). All values significant with p<0.001. See Appendix for details.
Tab. 2 - Correlazioni degli indici di grandine (ognuno riferito a singoli grelimetri) con le quote dei siti di misura (trend su 100 m di altitudine). Tutti i valori sono significativi con p<0.001. Consultare "Appendix" per i dettagli sugli acronimi.

4. CONCLUSIONS

This work highlighted a possible application of the processing of quantitative, impactometric high-resolution hail data collected in Trentino. The spatial analysis allowed to highlight geographic hail distribution. Even though a general increase of hail with elevation is evident (both as event occurrences and energetic intensity), altitude is not the only driver of hail, even in a small region like Trentino, where different areas show different degrees of exposure to hailstorms.

The other issue considered, the climatic link with lightning flashes recorded over the area (NLF), yielded a significant relationship between hail and electric activity of thunderstorm cells. In this case, too, there were differences between hail indices, each of them showing different statistical links with lightning. A good correlation was found between total accumulated energy (and its density, i.e., related to the covered area) and NLF. Being these indices the most useful in assessing the hail impact over an area, and being NLF easily measurable by the CESI-SIRF facility, we deem that NLF can be considered a good indicator of hail presence over a season. More careful inference should be used to investigate single episodes, as discussed in Section 1, owing to the time and space displacement of hail with respect to the lightning, and also to the different correlations with hail according to stroke polarity. However, this issue remains beyond the aims of this study. Since impactometric networks in the Alpine area risk to suffer a policy of dismantlement (or not implementing new ones), lightning recording seems a good candidate to become a proxy for hail amount. Of course, for a validation of the approach a wider area should be investigated than the one considered in this study.

Another potentially interesting aspect to be investigated in detail is the correlation between lightning activity and hail recorded at smaller scales. A validation of the findings of the quoted works would allow an extension of the results

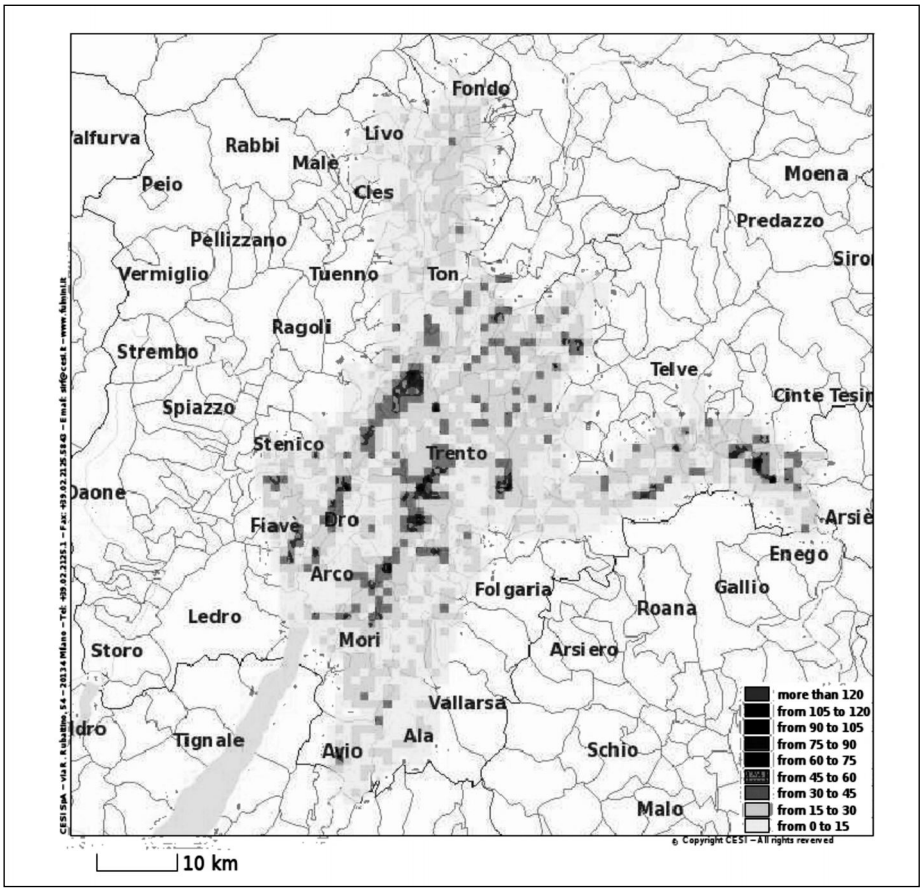

Fig. 6 - Total number of lightning flashes in the area corresponding to the coverage of the hail impactometric network (courtesy of CESI). Darker pixels correspond to higher flash rates.
Fig. 6 - Numero totale di fulmini nell'area coperta dalla rete impattometrica trentina (per gentile concessione di CESI). La tassellatura più scura corrisponde a valori più elevati di fulmini registrati.

down to the event scale. Positive results would make lightning survey, in association with other measurement devices (meteorological radar and raingauges), a feasible approach to indirect hail assessment.

ACKNOWLEDGEMENTS
Particular thanks to Amelia Caffarra (FEM) for her suggestions and to Luca Ghielmi (FEM) for calculating and editing the hail maps, and to Marina Bernardi (CESI) for supplying lightning data. We also wish to thank FEM's GIS Unit for the database management: Stefano Corradini, Alessandro Biasi, Danilo Caset, Ivan Piffer, Giambattista Toller, and above all Claudio Dalsant, who for over 30 years managed the collection and processing of hailpad measurements. We wish to thank the anonymous reviewer for his/her precious suggestions.

APPENDIX – Hail indices and units
cum_hit_surf_dens = accumulated hit surface density (=cum_hit_surf / total monitored surface) (-)
hail_days = nr. of hail days (or events: one event ≡ one hail day) (-)
m_surf_ev = mean surface for event (km^2)
cum_en_dens = density of accumulated kinetic energy ($J\ m^{-2}$)
m.en_rep = mean energy per report (one report ≡ one event at one site) ($J\ m^{-2}$)
sd_en = standard deviation of kinetic energy (per report) (J)
m_ev_en = spatial mean kinetic energy for event ($J\ m^{-2}$)
m_tot_en = total kinetic energy per season (MJ)
max_en_rep = max kinetic energy for report ($J\ m^{-2}$)
extr_en_rep = extreme (90^{th} percentile) kinetic energy for report ($J\ m^{-2}$)
extr_tot_en_ev = total kinetic energy for extreme (90^{th} percentile) annual event (MJ)
tot_en_max_ev = total kinetic energy for maximum annual event (MJ)
tot_en_extr_ev = total kinetic energy for extreme (90^{th} percentile) event (MJ)

REFERENCES
Berthet C., Dessens J., Sanchez J.L., 2010. Regional and yearly variations of hail frequency and intensity in France. Atmospheric Research, 100:391-400.

Berz G., and Siebert A., 2000. World of natural hazards. CD-ROM 302-02650, Münchener Rückversicherung.

Brunetti M., Maugeri M., Nanni T., and Navarra A., 2002. Droughts and extreme events in regional daily Italian precipitation series, International Journal of Climatology, 22:543–558.

Changnon S.A., 1992. Temporal relations between hail and lightning. Journal of Applied Meteorology, 31(6):587-604.

Coleman T., 2003: The impact of climate change on Insurance against catastrophes. Preprints of 2003 Biennial Convention of The Institute of Actuaries of Australia.

Dessens J., and Fraile R., 1994. Hailstone size distributions in southwestern France. Atmospheric Research, 33:57-73.

Eccel E., and Ferrari P., 1997. La grandine in Trentino: risultati dell'analisi climatologica per il ventennio 1974 - 1993. Quaderni di Esperienze & Ricerche n. 3 dell'Istituto Agrario di S. Michele, pp. 71.

Eccel E., and Saibanti, S., 2007. Inquadramento climatico dell'Altopiano di Lavarone-Vezzena nel contesto generale trentino. Studi Trentini di Scienze Naturali, Acta Biologica 82(2005):111-121.

Eccel E., Cau P., Riemann-Campe K., Biasioli F., 2012. Quantitative hail monitoring in an alpine area: 35 year climatology and links with atmospheric variables. International Journal of Climatology, 32:503-517. DOI: 10.1002/joc.2291.

Emersic C., Heinselman P.L., MacGorman D.R., Bruning E.C., 2011. Lightning Activity in a Hail-Producing Storm Observed with Phased-Array Radar. Monthly Weather Review, 139:1809-1825.

Fraile R., Berthet C., Dessens J., Sànchez J.L., 2003. Return periods of severe hailfalls computed from hailpad data. Atmospheric Research, Vol. 67– 68:189– 202.

Giaiotti D., Nordio S., and Stel F., 2003. The climatology of hail in the plain of Friuli Venezia Giulia. Atmospheric Research 67– 68:247– 259.

Grass Development Team, 2010. Geographic Resources Analysis Support System (GRASS) Software, Version 6.4.0. Open Source Geospatial Foundation. http://grass.osgeo.org

Hohl R., and Schiesser H.H., 2001. Cloud-to-ground lightning activity in relation to the radar-derived hail kinetic energy in Switzerland. Atmospheric Research, 56:375-396.

Manzato A., 2012. Hail in NE Italy: Climatology and bivariate analysis with the sounding-derived indices. Journal of Applied Meteorology and Climatology, *accepted*.

Meehl G.A., Stocker T.F., Collins W.D., Friedlingstein P., Gaye A.T., Gregory J.M., Kitoh A., Knutti R., Murphy J.M., Noda A., Raper S.C.B., Watterson I.G., Weaver A.J., Zhao Z., 2007. Global Climate Projections. In: Climate Change 2007: The Physical Science Basis. Contribution of Working Group I to the Fourth Assessment Report of the Intergovernmental Panel on Climate Change [Eds. Solomon S., Qin D., Manning M., Chen Z., Marquis M., Averyt KB., Tignor M., Miller HL]. Cambridge University Press, Cambridge, United Kingdom and New York, NY, USA.

Montefinale T., Ferrari P., Rafanelli C., and Paoletto P., 1982. Misure dell'attività grandinigena in provincia di Trento, periodo 1974-1982. Parte prima: calibrazione dei rilevatori di grandine al suolo. Esperienze & Ricerche, St. Speriment. Agraria Forestale di S. Michele all'Adige, Vol. 12:85-97.

Munich Re., 2000. Review of natural disasters 1999, Report No. 2946-Me, 2000.

R Development Core Team, 2011. R: A language and environment for statistical computing. R Foundation for Statistical Computing, Vienna, Austria. ISBN 3-900051-07-0, URL http://www.R-project.org/.

Sànchez J.L., Fraile R., DelaMadrid J.L., DelaFuente M.T., Rodriguez P., and Castro A., 1996. Crop damage: the hail size factor. Journal of Applied Meteorology, Vol. 35:1535-1541.

Schleusener R.A., and Jennings P.C., 1960. An energy method for relative estimates of hail intensity. Bull. Am. Meteorol. Society, Vol. 41, Nr. 7.

Soula S., Seity Y., Feral L., Sauvageot H., 2004. Cloud-to-ground lightning activity in hail-bearing storms. Journal of Geophysical Research – Atmospheres, 109. DOI: 10.1029/2003JD003669.

Sugier J., and Tabary P., 2006. Evaluation of dual-polarization technology at C-band for operational weather radar network. Report of the EUMETNET Opera 2, WPs 1.4 and 1.5, Deliverable b (available at http://www.knmi.nl/opera), 44 pp.

SwissRe 2006. The effect of Climatic Change: Storm damage in Europe on the rice, Focus Report, SwissRe, Switzerland.

Vinet F., 2001. Climatology of hail in France. Atmospheric Research, 56:309-323.

Implementation and validation of *Climak 3* weather generator

Alvaro Rocca[1], Oxana Bashanova[1], Fabrizio Ginaldi[1], Francesco Danuso[1]*

Abstract: *Weather generators (WG) are stochastic models, which generates series of weather data of indefinite length with statistical properties similar to those of the original series. WG have been extensively used in different biophysical models, providing them with meteorological input data.* Climak 3 *is a new version of* Climak *(Danuso, 2002), capable to generate daily meteorological data of precipitation, minimum and maximum air temperatures, solar radiation, reference evapotranspiration and wind speed. The performance of* Climak 3 *was tested using meteorological datasets coming from different locations over the world. The results for Italy, Bulgaria and Argentina are presented and discussed.*
Keywords: *weather generators, stochastic models, validation, climate change.*

Riassunto: *I generatori climatici (WG) sono modelli stocastici in grado di produrre serie climatiche di lunghezza indefinita, con caratteristiche statistiche simili a quelle delle serie storiche originali. I WG sono ampiamente utilizzati per generare dati meteorologici input per diversi modelli biofisici.* Climak 3 *è una nuova versione di generatore* Climak*, che è in grado di generare dati meteorologici giornalieri di precipitazioni, temperatura minima e massima dell'aria, radiazione solare, evapotraspirazione e velocità del vento. La capacità del modello di ricreare le caratteristiche climatiche è stata testata su diversi siti. Si riportano i risultati per Italia, Bulgaria e Argentina.*
Parole chiave: *generatori climatici, modelli stocastici, validazione, cambiamenti climatici.*

INTRODUCTION

Climate is one of the main factors which affect human activities and different ecological processes. Great efforts have been devoted to weather forecasting investigations. The study of the climate statistical properties has allowed the development of climatic stochastic models (weather generators) for the generation of weather data (Jones *et al.*, 1970; Richardson, 1981; Larsen and Pense, 1982; Shu Geng *et al.*, 1985; Richardson and Nicks, 1990; Semenov *et al.*, 1998; Donatelli *et al.*, 2005; Donatelli *et al.*, 2009; Birt *et al.*, 2010). Weather generators (*WG*) are stochastic models, which produce meteorological data of indefinite length, on the base of climatic parameters estimated from historic meteorological data series. Application of weather generators allows Monte Carlo simulations to obtain probability distributions of agro-ecological variables related to climate, spatial interpolation of the climate parameters (thus obtaining data for locations not covered by meteorological stations) and assessment of environmental scenarios depending on climatic changes.

In this paper the third version of the *Climak* (Danuso and Della Mea, 1994; Danuso *et al.*, 2011) weather generator is presented. *Climak* was developed in the early '90s and provided significant results (Acutis *et al.*, 1999; Danuso, 2002). Initially *Climak* generated daily data of precipitation, maximum and minimum temperatures, solar radiation and evapotranspiration. The new version (*Climak 3*), developed jointly with the weather generator CLIMA (Donatelli *et al.*, 2005; Donatelli *et al.*, 2009), allows also the generation of wind speed data. This version has been developed and implemented using the SEMoLa language (Danuso, 2003). To validate *Climak 3*, generated meteorological data series were compared with the historical ones.

MATERIALS AND METHODS

Model description

Climak 3 has a structure similar to other weather generators (Jones *et al.*, 1970; Richardson, 1981; Larsen and Pense, 1982; Shu Geng *et al.*, 1985; Richardson and Nicks, 1990; Semenov *et al.*, 1998; Donatelli *et al.*, 2005; Donatelli *et al.*, 2009; Birt *et al.*, 2010). It generates daily total precipitation (*Prec*), daily minimum and maximum air temperatures (*Tmin, Tmax*), daily integral of solar radiation (*Rg*), evapotranspiration (*ETr*) and daily wind speed (*Winds*) (Tab. 1). For the evapotranspiration, this could be generated from real measured evapotranspiration or from

* Corresponding Author: e-mail: francesco.danuso@uniud.it
[1] Dipartimento di Scienze Agrarie e Ambientali, Università di Udine, Udine, Italy
Received 28 October 2011, accepted March 2012.

Meteorological variable	Abbreviation	Unit	Model parameters*
Precipitation	*Prec*	mm	Pdd_i, Prd_i; Ag_i, Bg_i
Minimum temperature	*Tmin*	°C	A_i, B_i, C_i, D_i, E_i; Rn_i, SRn_i ; $RRnn_i$
Maximum temperature	*Tmax*	°C	A_i, B_i, C_i, D_i, E_i; Rx_i, SRx_i; $RRnx_i$
Solar radiation	*Rg*	MJ/m²·d	b_0, b_1; Ab_i, Bb_i
Evapotranspiration	*Etr*	mm	a_0, a_1, S_{etr} ; c_0, c_1, S_{etp} , d_0,d_1
Wind speed	*Winds*	m/s	bw_0, bw_1, bw_2, bw_3, bw_4, bw_5; Rw

*i – month; see text for the meaning of the symbols

Tab. 1 - Meteorological variables considered by *Climak 3*.
Tab. 1 - Variabili meteorologiche considerati in Climak 3.

calculated potential or reference evapotranspiration (Allen *et al*., 1998), depending on which type of evapotranspiration parameters have been estimated. The weather generation procedure consists of 1) estimation of climatic parameters from historical meteorological data, and 2) data generation based on the statistical parameters obtained (Fig. 1). In *Climak 3* precipitation are not distinguished between solid (hail, snow) and liquid (rain) precipitation.

As a first step, *Climak 3* generates the occurrence of rainy or dry day and the rainfall amount, if the day is rainy. After rainfall generation, minimum and maximum air temperatures are generated, separately, for rainy and dry days. Solar radiation is obtained from the astronomical photoperiod (*Ph*) and from the daily thermal excursion. The evapotranspiration is generated from the solar radiation data; if data of solar radiation are not

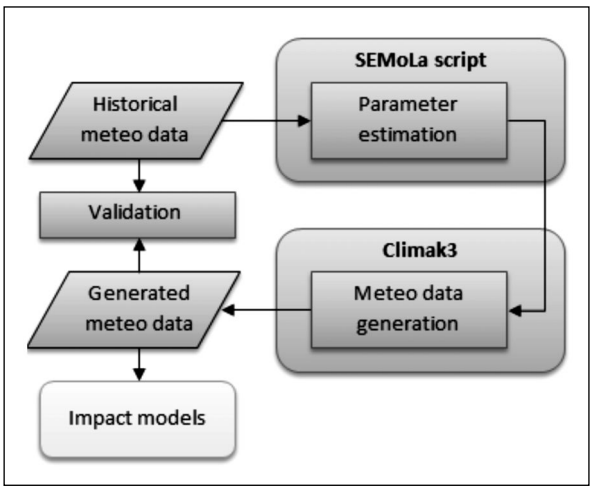

Fig. 1 - Application of the *Climak 3* weather generator.
Fig. 1 - Applicazione del generatore climatico Climak 3.

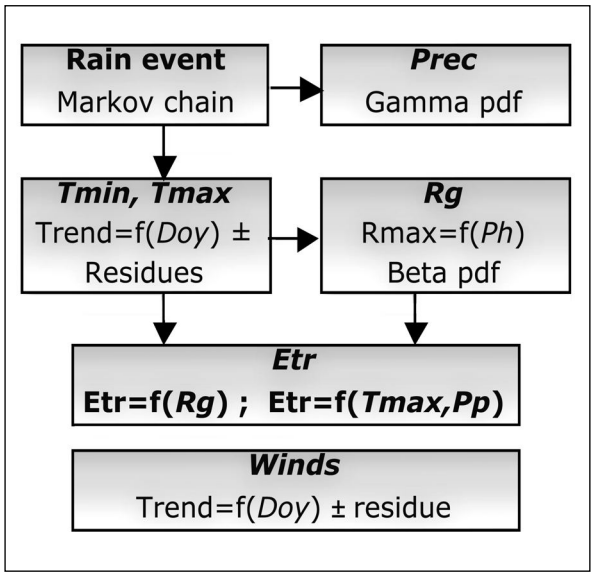

Fig. 2 - Procedure of generation of meteorological variables.
Fig. 2 - Procedura di generazione delle variabili meteorologiche.

available, evapotranspiration is obtained from photoperiod and maximum temperature. In the end, wind speed values are generated (Fig. 2).

The state of the day (rainy or dry), being a stochastic process, is represented by a first order Markov chain according to the dry to dry (*Pdd*), rainy to dry (*Prd*), dry to rainy (*Pdr*) and rainy to rainy (*Prr*) transition probabilities. The transition probabilities parameters were previously estimated from historical date, for each month, as:

$$Pdd = Ndd/Nd \quad Pdr = 1 - Pdd \;;$$
$$Prd = Nrd/Nr \quad Prr = 1 - Prd$$

where:

Ndd number of dry days in the month preceded by a dry day

Nd total number of dry days in the month
Nrd number of dry days in the month preceded by a rainy day
Nr total number of rainy days in the month

The rain event is generated by sampling, for each day, a random value from the uniform distribution $U(0,1)$. If the current day is dry, the *Pdd* probability is used; if the sampled value $U(0,1)$ is less than *Pdd* the following day is set to "dry", otherwise it is set to "rainy". The same procedure is adopted with the *Prd* transition probability if the present day is rainy. The considered probabilities are specific for each month.
If the day is at a rainy status the rainfall amount (*Prec*) is sampled from a Gamma probability density function, considering the threshold value of the instrumental sensitivity (*Sthr*, usually 0.2 mm):

$$Prec = \Gamma(A_g, B_g)$$

where A_g and B_g are the parameters, specific for each month estimated from historical date.

After rainfall generation, the minimum and maximum temperatures are generated separately, considering the status of the day (rainy or dry):

$$Temperature = Trend + Residue$$

where *Trend* is an average daily minimum/maximum temperature for the dry/rainy days, obtained as a function of the date, by interpolating a second order Fourier series:

$$Trend = A + B \cdot sin\left[(Doy - C) \cdot \frac{2\pi}{365}\right] + D \cdot sin\left[(Doy - E) \cdot \frac{4\pi}{365}\right]$$

A average annual minimum temperature (°C);
B semi-amplitude of the first term (°C);
C phase shift for the first term (days);
D semi-amplitude of the second term (°C);
E phase shift for the second term (days);
Doy day of the year (from 1 to 365 or 366).

Parameters *C* and *E*, estimated from historical data, are considered constant for all years because of the small variability observed, while means and standard deviations of *A*, *B* and *D* parameters are different in relation to the year and for the minimum/maximum and rainy/dry temperature combinations (*Tmin* trend for dry days, *Tmax* trend for dry days, *Tmin* trend for rainy days, *Tmax* trend for rainy days). These parameters were estimated by linear regression of the trend function (after linearization) of the observed temperatures vs. day of the year. Thus, for each year the annual trends of minimum and maximum air temperature on dry and rainy days are calculated.
During generation these parameter were used for sampling from the normal probability distributions $N(MA,SA)$, $N(MB,SB)$ and $N(MD,SD)$ (where *MA*, *MB* and *MD* are the mean values of *A*, *B* and *D*; *SA*, *SB* and *SD* are the standard deviations) at the beginning of each new year.
After the generation of the trend, month by month, temperature is generated by adding the *Residue* to the trends obtained. Residues for minimum temperature (*Rn*), specific for each month, are sampled from the autocorrelated normal distribution with mean zero and standard deviation *SRn*:

$$Rn = RRnn \cdot R1_n + SRn \cdot \cdot \sqrt{1 - RRnn^2} \cdot N(0,1)$$

where *RRnn* is the autocorrelation coefficient, $R1_n$ the residue of minimum temperature of the previous day, already generated and $N(0,1)$ the value sampled from a normal distribution with 0 mean and 1 standard deviation.
Residues for maximum temperature (*Rx*), also specific for each month, are sampled from the bivariate normal distribution with mean 0, standard deviation *SRx* and correlation coefficient *RRnx*, depending on the value of the minimum temperature residue *Rn*:

$$Rx = \frac{RRnx \cdot SRx \cdot Rn}{SRn} + SRx \cdot \cdot \sqrt{1 - RRnx^2} \cdot N(0,1)$$

SRn, *RRnn*, *SRx* and *RRnx* parameters were estimated from the historical date.
Daily solar radiation is calculated on the base of the air temperature excursion as:

$$Rg = Rmax \cdot Rr$$

where *Rmax* is the annual trend of the maximum daily radiation, linearly related to the duration of

the photoperiod (*Ph*) and considered constant for each day of the year. This is performed with the method described in Keisling (1982). The parameters of the linear relation between *Rmax* and *Ph* are obtained by selecting only the maximum values of the solar radiation in ten-day periods of the year.

$$Rmax = b_1 \cdot Ph + b_0$$

The ratio of the daily radiation and maximum radiation (*Rr=Rg/Rmax*) is the atmosphere transmittance, which varies from 0 to 1. This ratio is then divided into five air temperature excursion classes, within which it is found to be distributed according to the Beta probability distribution function (*pdf*), with parameters A_b and B_b, estimated from historical datasets.
For each class and from the ratio *Rr* the two parameters of the Beta distribution are estimated, using the moments:

$$A_b = M^2 \cdot \frac{1-M}{V} - M$$

$$B_b = A_b \cdot \frac{1-M}{M}$$

where *M* and *V* are the mean and variance of *Rr*, for each excursion class. After rainfall generation, the minimum and maximum temperatures are generated separately, considering the status of the day (rainy or dry).
The evapotranspiration shows the well-known good linear relation with the radiation (Doorembos and Pruitt, 1977); less good is that one with maximum air temperature and photoperiod. Since radiation data are often not available in the historical meteorological datasets, two different approaches for the evapotranspiration generation are adopted. The first one if radiation is available with a more precise generation and the second using temperature and photoperiod:
1) With solar radiation data available: daily evapotranspiration is obtained as a linear function of the daily radiation (*Rg*) plus a residue obtained from a normal distribution (unique for all the months) with standard deviation *Setr*:

$$ETr = a_1 \cdot Rg + a_0 + N(0, Setr)$$

2) If radiation data are not available: daily evapotranspiration is generated as a function of maximum air temperature (*Tmax*) and photoperiod (*Ph*):

$$Etr = c_1 \cdot Tmax \cdot Ph^2 + c_0 + N(0, Setp)$$

where *Setp* is the standard deviation of the residues, related to the photoperiod by a linear function, $Setp=d_1 \cdot Ph + d_0$.
Wind speed variability has been often expressed using Weibull density function (Takle and Brown, 1977; Weisser and Foxon, 2003; Aksoy *et al.*, 2004; Bhattacharya, 2010). This approach is applied widely and considered as a standard. Despite this, Weibull probability density function is not able to properly represent the minimum values of wind speed (Weisser and Foxon, 2003). Moreover, this approach is not able to correctly describe the annual trend and the monthly distribution of the historical data.
To address these limitations, in *Climak 3*, a new approach for generating wind speed data was implemented. Daily data of average wind speed (*Winds*) are generated considering four aspects defined through the analysis of meteorological series: wind speed data have an asymmetric distribution (of a logarithmic type), the historical records show the presence of an annual trend, the residues distribution vary from month to month and resulted to be auto-correlated with those of previous days. Thus, the model of wind generation was developed using logarithmically transformed data interpolating the trend with a third-degree polynomial function:

$$LWs = bw_0 + bw_1 \cdot Doy + bw_2 \cdot \cdot Doy^2 + bw_3 \cdot Doy^3$$

where $bw_0, \ldots bw_3$ are the parameters, estimated based on historical data. Then, the wind speed data are obtained as:

$$Winds = \exp(LWs + Rw)$$

Rw is the residue from trend, obtained from the bivariate normal distribution of residues, autocorrelated with the residue of the previous day.
In the weather generator, different types of pseudo-random number generators can be used: a simple but faster LCG (linear congruential generator) or the Mersenne Twister series (32, 53 or 64 bit) having a longer period (Matsumoto and Nishimura, 1998). The 32 bit Mersenne Twister pseudo-random number generator has a period of $(2^{19937}-1)$. The procedures for parameter

State/Region	Latitude (°)	Longitude (°)	Elevation, ma.s.l.	Ecoregion division
Italy, Friuli V.G.	46.00	13.00	100	Mediterranean
Bulgaria, Vratsa	43.23	23.52	115	Moderately continental
Argentina, La Pampa	-36.25	-63.50	119	Subtropical

Tab. 2 - Geographical coordinates and elevation of the study areas.
Tab. 2 - Coordinate geografiche e altitudine delle aree di studio.

estimation and model validation are implemented as scripts of the SEMoLa framework. Both are completely open, easy to modify and freely available.

Case study

The performance of *Climak 3* was evaluated using meteorological datasets from different locations of Europe and South-America. Relatively long records of daily weather variables (minimum and maximum air temperature, precipitation, solar radiation, evapotranspiration) were provided by Joint Research Center (EU) and Regional Meteorological Service of the Friuli Venezia Giulia region (OSMER). Wind speed data were available only in datasets from Italy. This data allowed to test *Climak 3* performance in different climatic conditions. In this paper, results for mediterranean, moderately continental and subtropical austral climates are presented. The datasets from meteorological stations of Italy, Bulgaria and Argentina were used (Fig. 3). The chosen sites are characterized by different meteorological conditions (Tab. 2). The number of years of the data ranged from 10 for Italy to 20 for Argentina and 35 for Bulgaria.

Validation

The goodness of generated weather data depends on the model itself and the quality of the parameters estimation. This, in turn, depends on the calculation methods and on the number of years of historical data available. Weather generators are supposed to generate synthetic weather series with statistical properties similar to the observed ones (Semenov *et al.*, 1998; Donatelli *et al.*, 2005). This means that: (i) means and variances of daily synthetic weather data are to be not significantly different from those of observed series, (ii) means and variances of monthly values of the weather variables from synthetic and observed series are to be comparable, (iii) synthetic weather series are to follow the probability distribution statistically not different from the historical ones.

To test the performance of *Climak 3* a validation procedure has been developed. The procedure consists of different graphical analysis evaluating the correspondence of historical and generated data (Semenov *et al.*, 1998; Hayhoe, 2000; Birt *et al.*, 2010), comparing monthly means and monthly standard deviations of all meteorological variables. Rainfall was also compared using relative frequency histograms. Cumulative probability functions were used for graphical representation of the correspondence between historical and generated data distribution.

Validation was performed using generated datasets of 100 years. A long synthetic series provided stable statistical properties thus ensuring that any significant difference between the observed series and the synthetic series is not a result of sampling, as the observed series is only a part of the 'real' stochastic process (Qian *et al.*, 2004).

Quantile-quantile (QQ) plots are also used to demonstrate visually how well the generated series followed the probability distribution of the observed

Fig. 3 - Study areas geographical position.
Fig. 3 - Posizione geografica delle aree di studio.

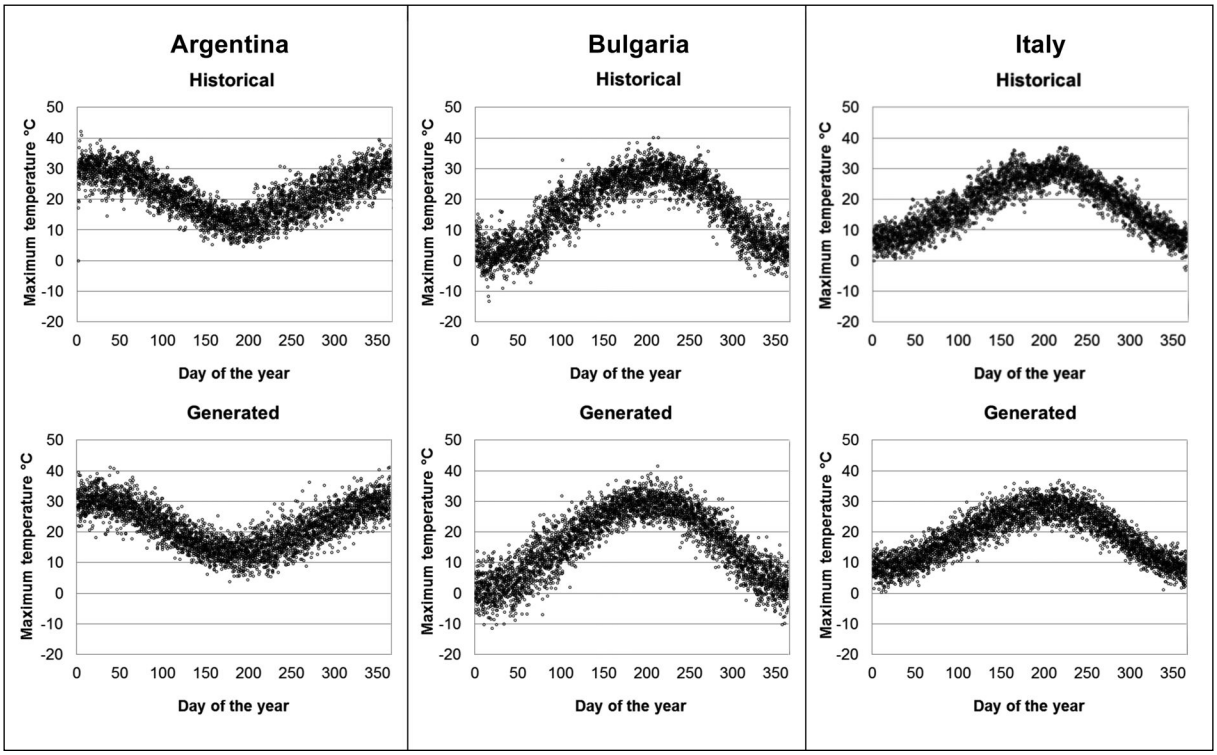

Fig. 4 - Daily maximum air temperature (°C) for historical and generated data for Argentina, Bulgaria and Italy.
Fig. 4 - Temperatura massima giornaliera (°C) storica e generata per Argentina, Bulgaria e Italia.

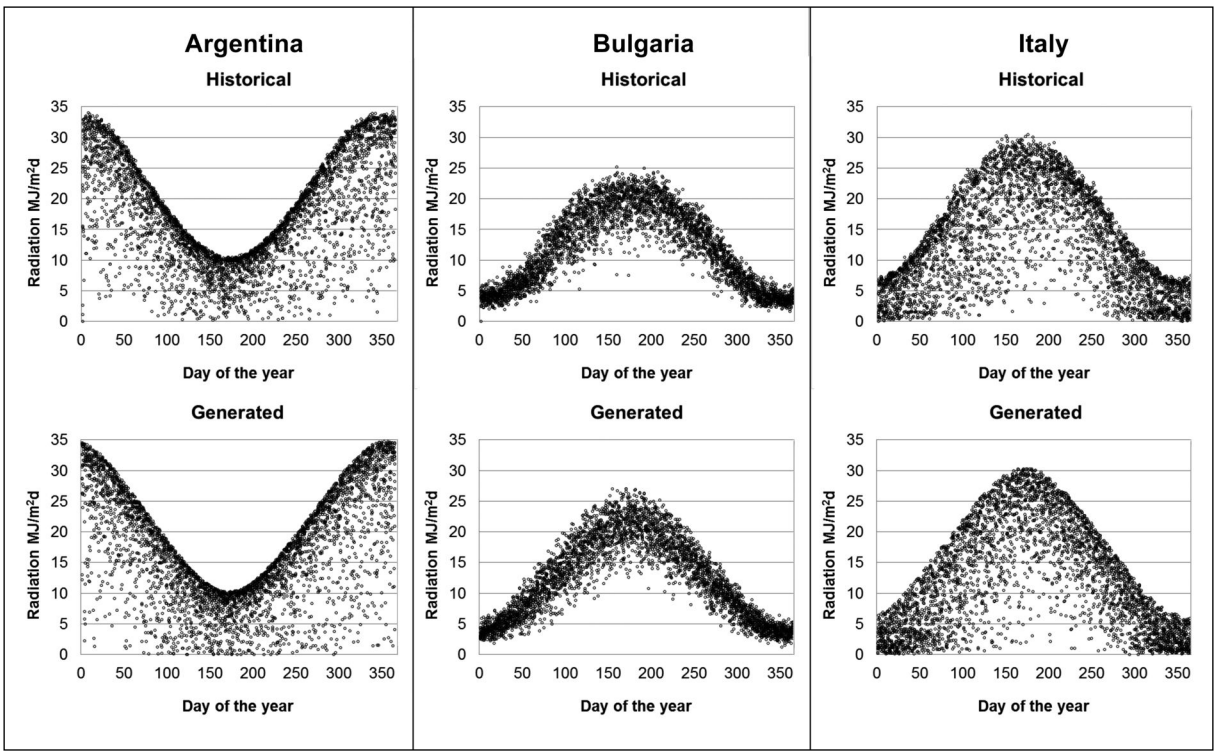

Fig. 5 - Daily solar radiation (MJ/m²/d) for historical and generated data for Argentina, Bulgaria and Italy.
Fig. 5 - Radiazione solare giornaliera (MJ/m²/d) storica e generata per Argentina, Bulgaria e Italia.

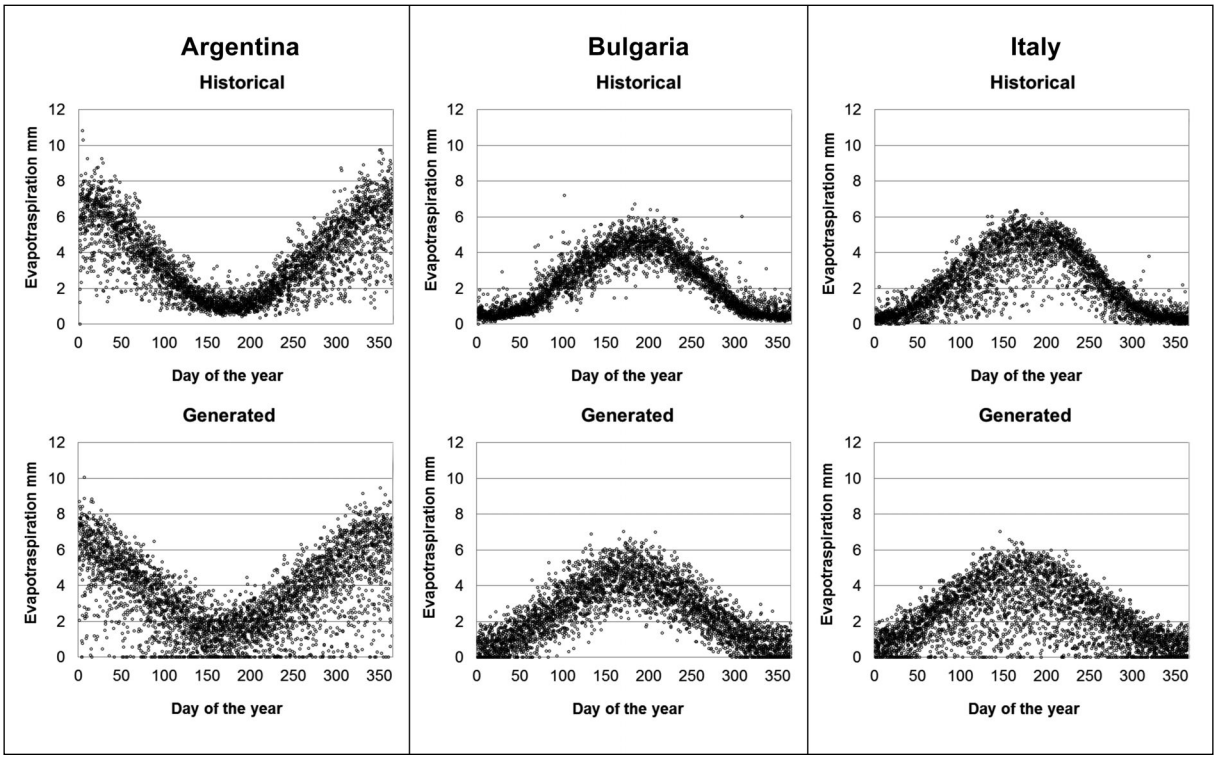

Fig. 6 - Daily reference evapotranspiration (mm) for historical and generated data for Argentina, Bulgaria and Italy.
Fig. 6 - Evapotraspirazione di riferimento giornaliera (mm) storica e generata per Argentina, Bulgaria e Italia.

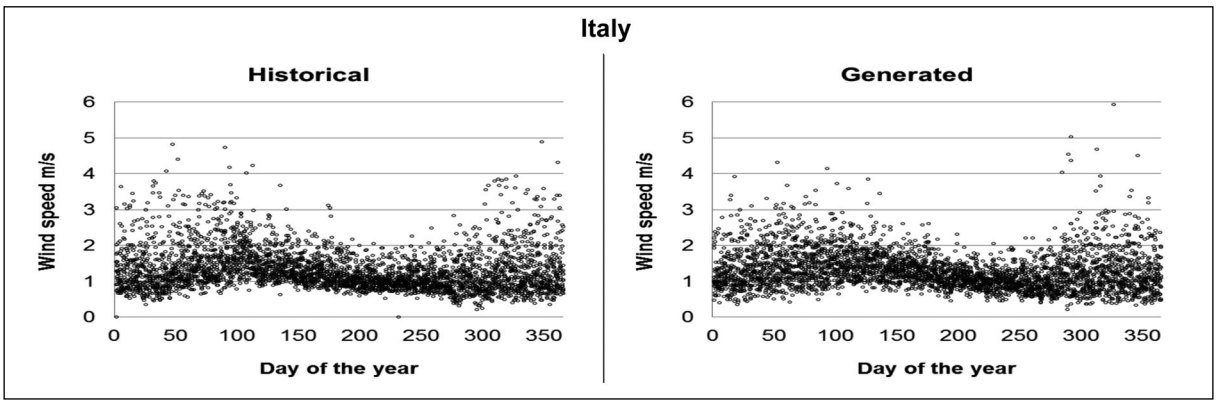

Fig. 7 - Daily average wind speed (m/s) of historical and generated data for Italy.
Fig. 7 - Velocità del vento media giornaliera (m/s) storica e generata per l'Italia.

series (Qian *et al.*, 2004), for daily minimum and maximum temperature, radiation, wind speed and precipitation. Rain data include only the values between the 10th and the 90Th quantile of the distribution to not consider extreme values.

RESULTS AND DISCUSSION

Using *Climak 3*, meteorological datasets for different locations were generated. It was expected that the software implementation of *Climak 3* would provide realistic output data for different climatic conditions. In Figg. 4, 5 and 6 the results for Italy, Bulgaria and Argentina are presented. In Fig. 7 historical and generated data of wind speed (m/s) are presented only for Italy. From these figures of daily data comparison it is possible to notice that *Climak 3* gives satisfactory results. In general, the annual trend of all

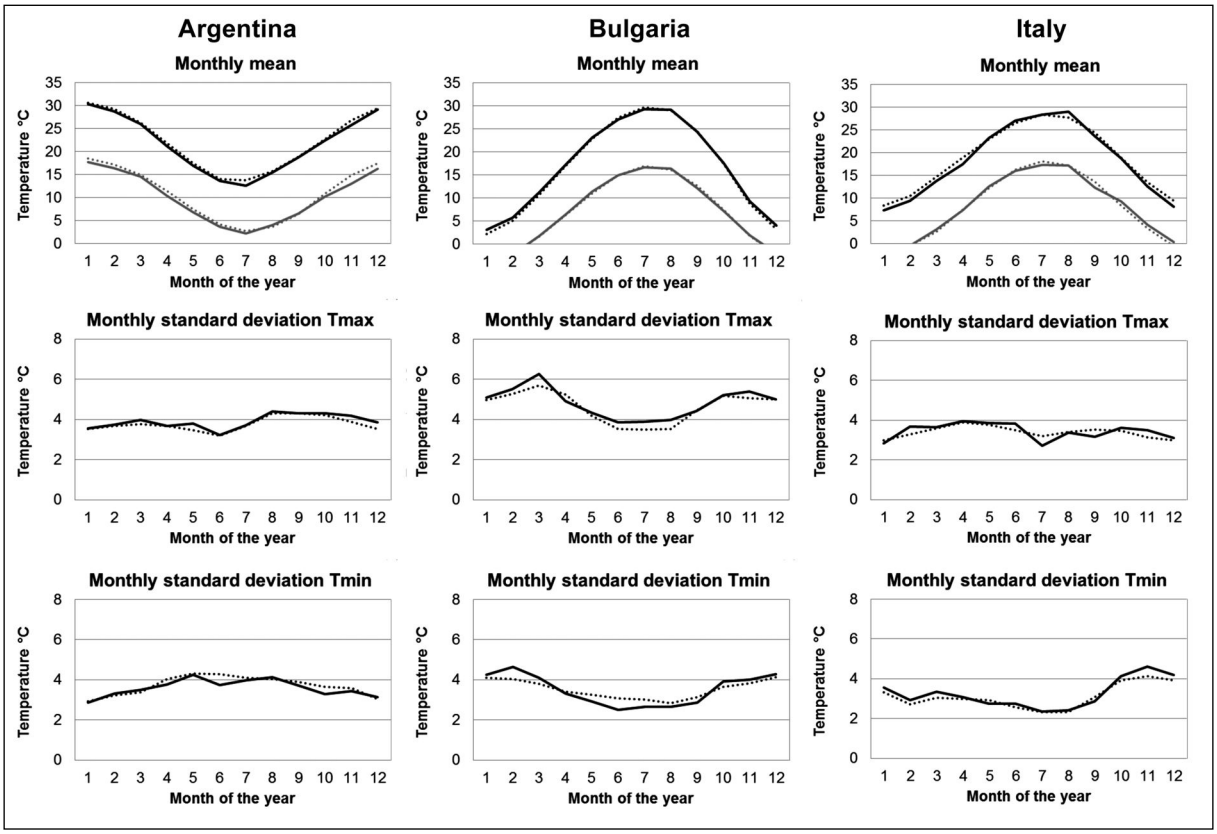

Fig. 8 - Monthly mean and standard deviation of maximum and minimum temperatures (°C) for historical and generated data for Argentina, Bulgaria and Italy.
Fig. 8 - Media mensile e deviazione standard della temperatura massima e minima (°C) storica e generata per Argentina, Bulgaria e Italia.

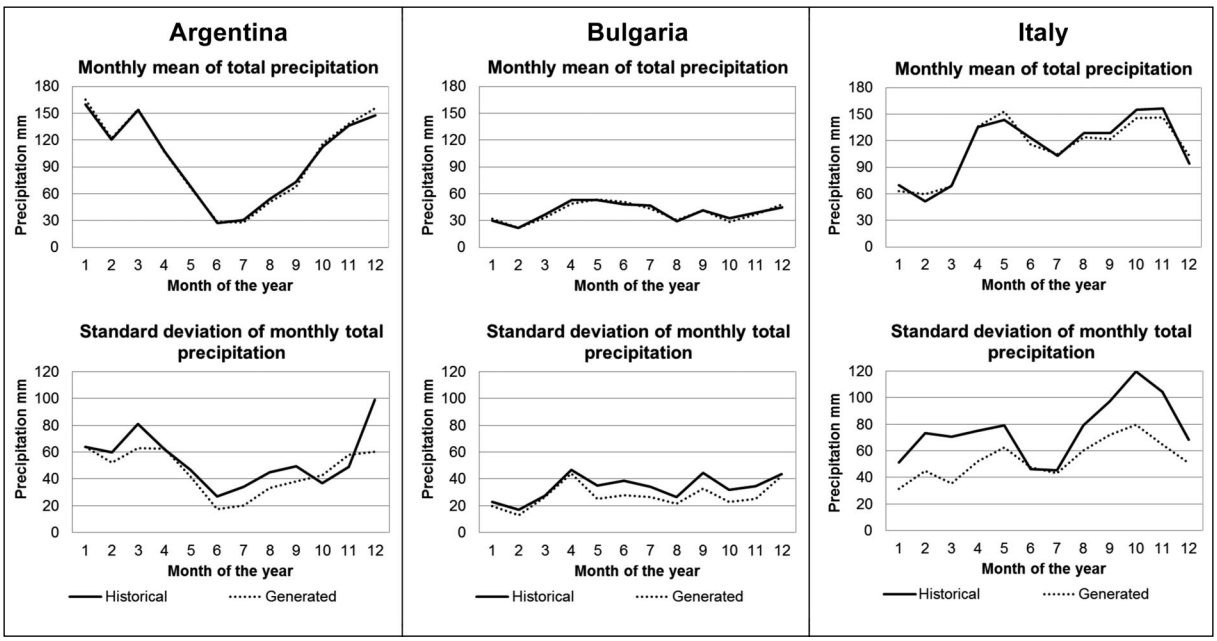

Fig. 9 - Monthly mean and standard deviation of precipitation (mm) of historical and generated data for Argentina, Bulgaria and Italy.
Fig. 9 - Media mensile e deviazione standard delle precipitazioni (mm) storiche e generate per Argentina, Bulgaria e Italia.

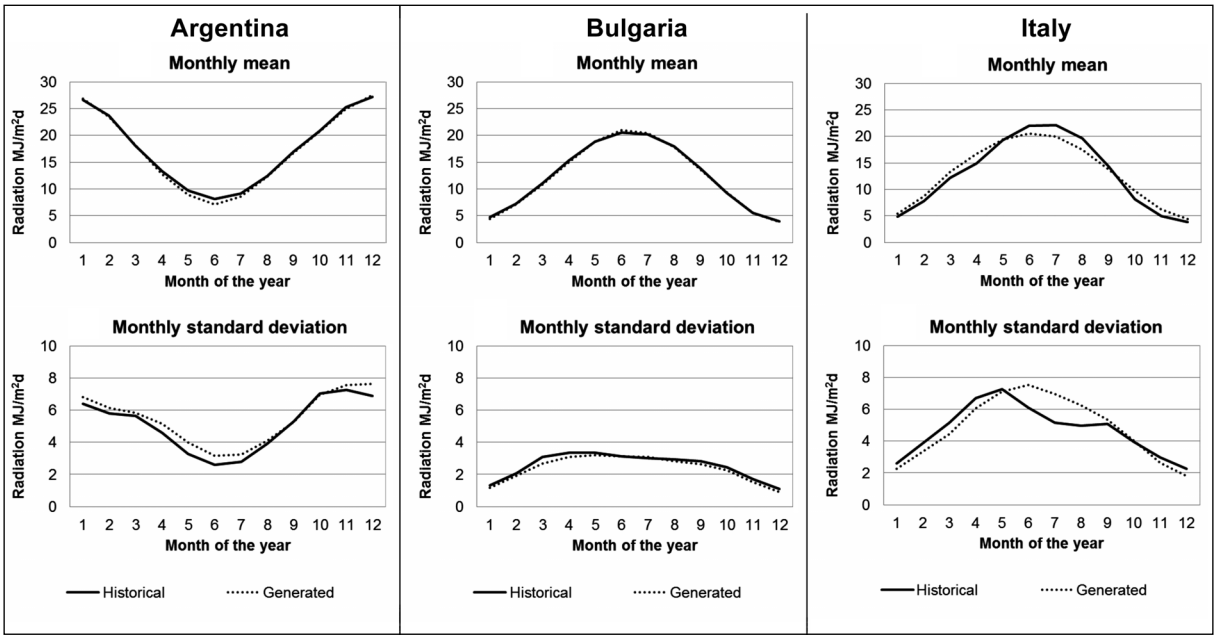

Fig. 10 - Monthly mean and standard deviation of solar radiation (MJ/m^2) of historical and generated data for Argentina, Bulgaria and Italy.
Fig. 10 - Media mensile e deviazione standard della radiazione solare (MJ/m^2) storica e generata per Argentina, Bulgaria e Italia.

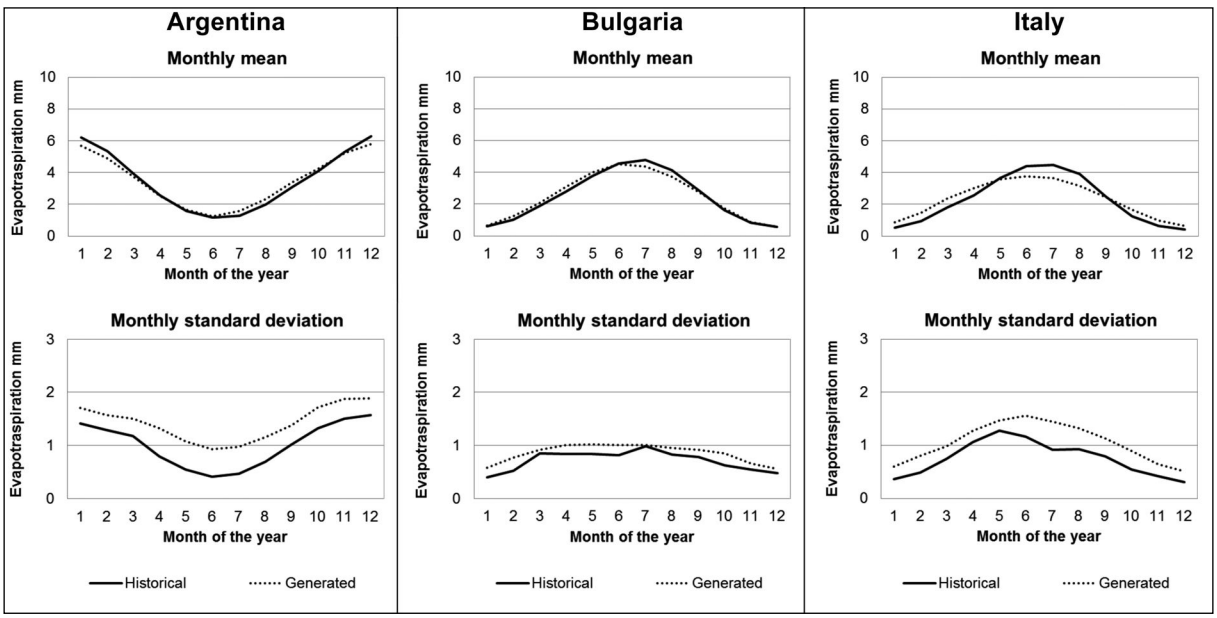

Fig. 11 - Monthly mean and standard deviation of reference evapotranspiration (mm) for historical and generated data for Argentina, Bulgaria and Italy.
Fig. 11 - Media mensile e deviazione standard dell' evapotraspirazione di riferimento (mm) storica e generata per Argentina, Bulgaria e Italia.

variables is followed. However in the generated data there is a slight overestimation of the evapotranspiration standard deviations, which can be neglected since the difference between values does not exceed 1 mm.

Results of monthly means and standard deviations comparison of meteorological variables are presented in Figg. 8, 9, 10, 11, 12. These figures confirm a good fitness of the synthetic and historical data, thus proving a good performance of *Climak 3*

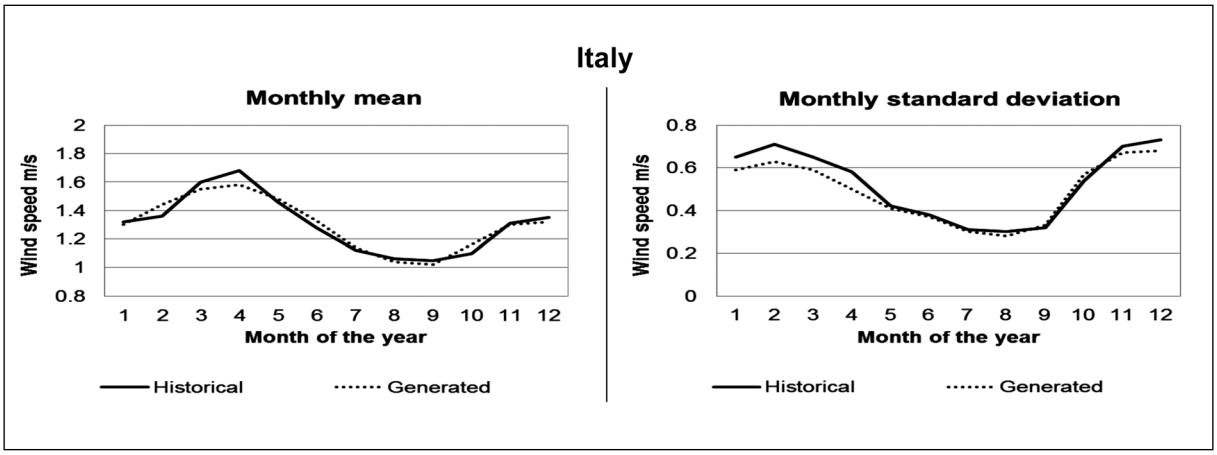

Fig. 12 - Monthly mean and standard deviation of wind speed (m/s) for historical and generated data for Italy.
Fig. 12 - Media mensile e deviazione standard della velocità del vento(m/s) storica e generata per l'Italia.

in generation of mean values and variability, though there is a slight shift, especially when representing rain and evapotranspiration variability. In Fig. 13 precipitation frequency histograms are presented.
From the Fig. 14, where cumulative distributions of maximum, minimum temperatures and precipitation for January and July are reported; it is possible to notice that in January for both hemispheres, variation ranges of maximum and minimum temperatures of the observed data is wider than those of generated ones.
In figure 15 the QQ plots are represented for daily minimum and maximum temperature, radiation, wind speed (only for Italy) and precipitation.

CONCLUSIONS

The goodness of a weather models basically depends on the model structure itself, on methods and algorithms applied for parameter estimation and on algorithms for data generation (sampling from probability distribution function). Validation results obtained show that *Climak 3* can be considered as sufficiently accurate tool for the generation of meteorological data in temperate and cold climates. In general, the behavior of the model has been satisfactory but some aspects are still to be improved. A new version *Climak 4* is now under development that will address these limitations introducing new algorithms for temperatures and radiation.
The further works will be focused on the improvement of the estimation and/or generation procedures of evapotranspiration and radiation data, and on a better representation of the *Tmax* and *Tmin* variability. Moreover, it will be necessary to develop issues concerning downscaling of meteorological variables and the

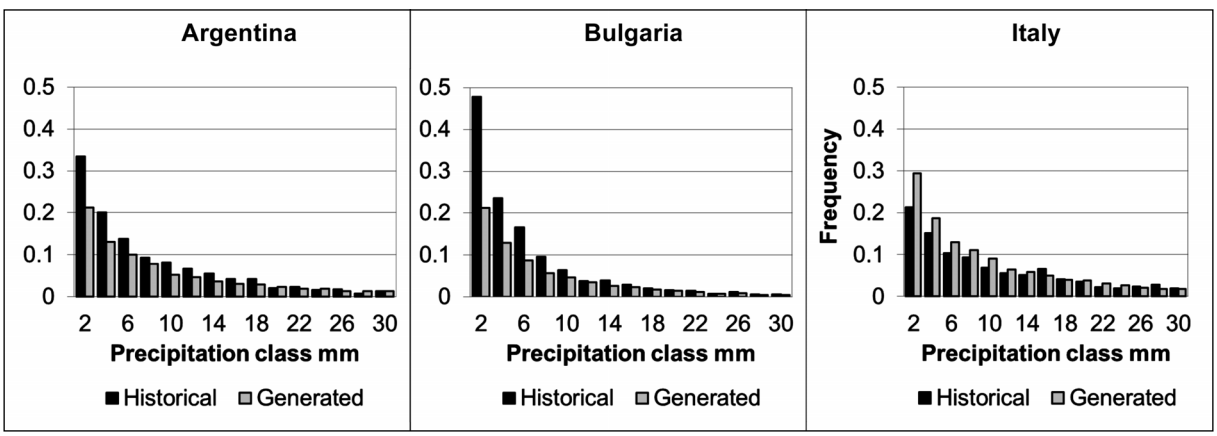

Fig. 13 - Precipitation frequency histograms (mm) for historical and generated data for Argentina, Bulgaria and Italy.
Fig. 13 - Istogrammi di frequenza delle precipitazioni storiche e generate per Argentina, Bulgaria e Italia.

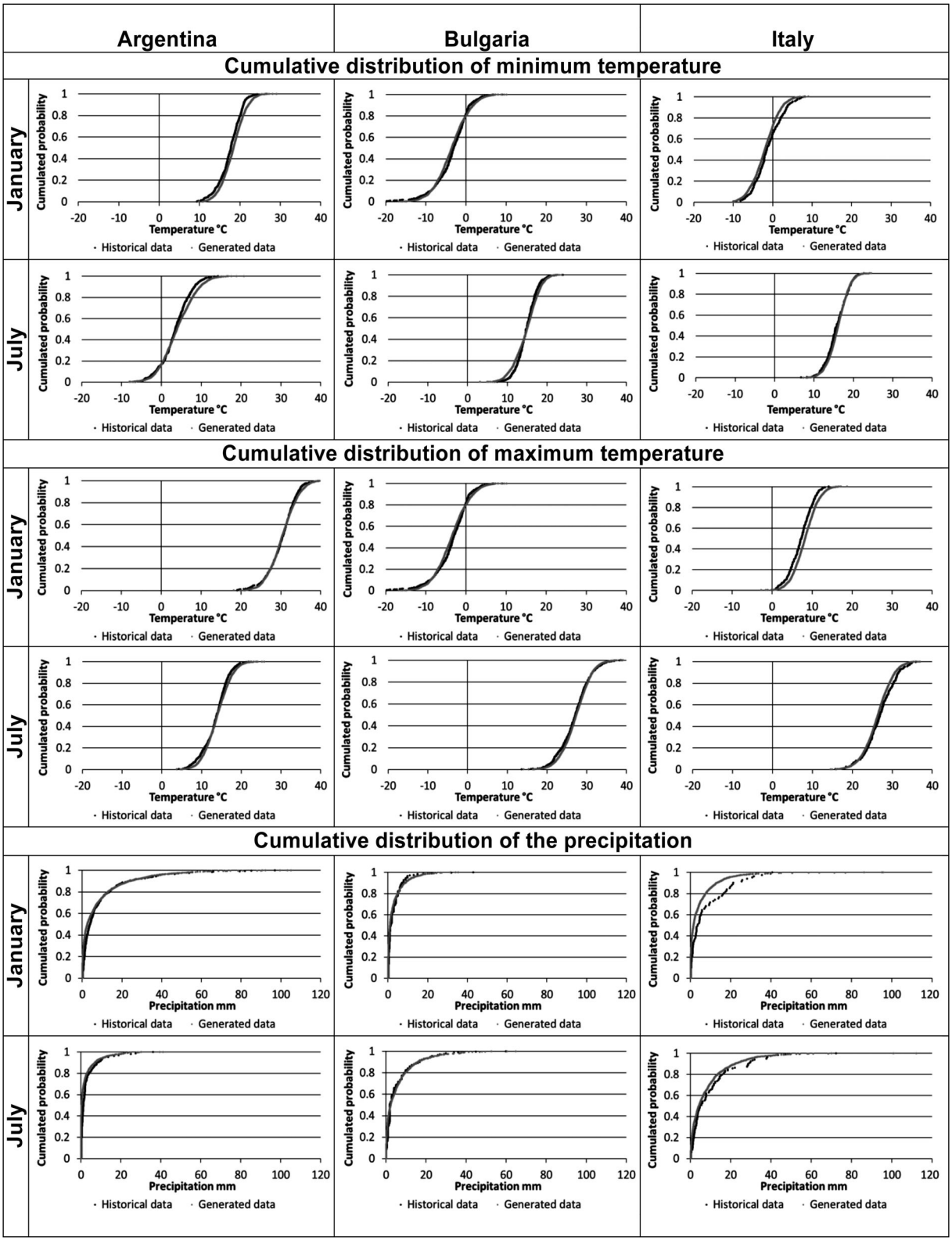

Fig. 14 - Comparison of cumulative distributions of maximum, minimum temperatures and precipitation for historical and generated data (only for the months of January and July) for Argentina, Bulgaria and Italy.
Fig.14 - Confronto delle distribuzioni cumulate delle temperature massime, minime e delle precipitazioni per dati storici e generati (solo per i mesi di Gennaio e Luglio) per Argentina, Bulgaria e Italia.

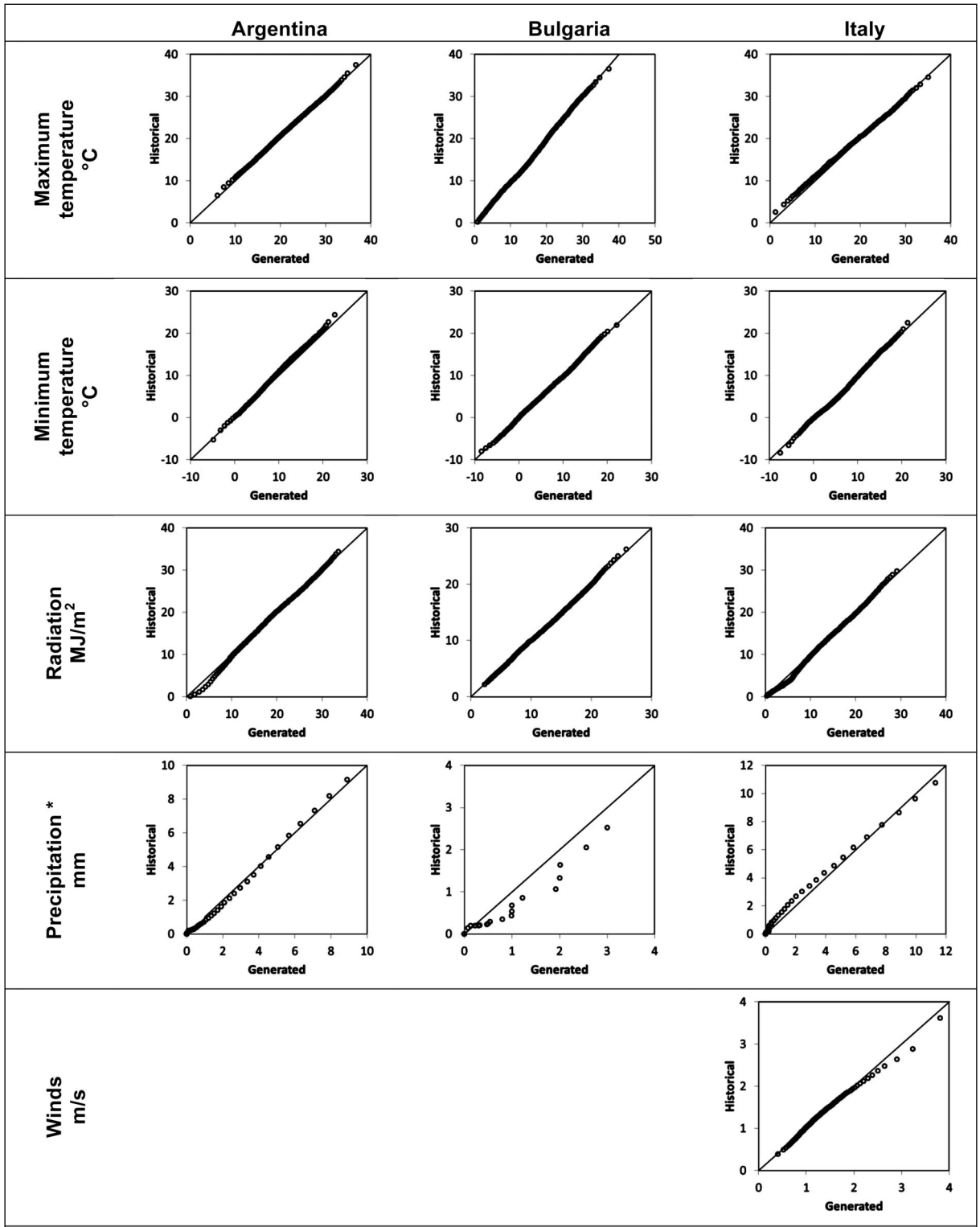

Fig. 15 - Quantile–quantile plot of maximum, minimum temperatures, radiation, precipitation and wind for historical and generated data for Argentina, Bulgaria and Italy.

Fig. 15 - Quantile – quantile plot delle temperature massime, minime, radiazione, precipitazioni e vento per dati storici e generati per Argentina, Bulgaria e Italia.

generation of extreme events, especially for precipitation and wind speed. In fact, wind speed model, at present, is not able to represent high speed values, observed in some locations.
Furthermore, a stand-alone application tool with easy to use graphical interface (*Climak WG*) is being developed in order to allow a simpler use of the weather generator.
Future developments will include also the generation of hourly data (Fatichi *et al.*, 2011).

Parameter estimation script, generation model and validation procedure are freely available from authors. The executable and source code of *Climak 3*, the script for the parameters estimation and that for the validation procedure are freely available from the web (http://www.dpvta.uniud. it/~Danuso/docs/Climatica/Climatica_Home.html).

ACKNOWLEDGEMENTS
Authors would like to acknowledge the JRC (Joint Research Center – European Commission) and the Regional Meteorological Services of the FVG region (OSMER) for availability of the meteorological data. Discussion and suggestions from Marcello Donatelli and Roberto Confalonieri have been particularly useful. This research has been funded by the Friuli Venezia Giulia region, in the framework of the project "Filiere agroenergetiche in FVG: valutazione economica energetica e ambientale" - L.R. N. 26 10.11.2005.

REFERENCES
Acutis M., Donatelli M. and Stockle C., 1999. Performances of two weather generators as a function of the number of available years of measured climatic data. Proc. 1th Int. Symp. Modelling Cropping Systems, 21-23 June, Lleida, Spain, 129-130.

Aksoy H., Fuat Z.T., Aytek A. and Unal E.N., 2004. Stochastic generation of hourly mean wind speed data. Renewable Energy, 29: 2111-2131.

Allen R.G., Pereira L.S., Raes D., Martin Smith M., 1998. Crop evapotranspiration - Guidelines for computing crop water requirements - FAO Irrigation and drainage paper 56. FAO - Food and Agriculture Organization of the United Nations. Rome, 1998.

Bhattacharya P., 2010. A study on a Weibull distribution for estimating the parameters. Journal of Applied Quantitative methods, 5 (2): 234-241.

Birt A.G., Valdez-Vivas M.R., Feldman R.M., Lafon C.W., Cairns D., Coulson R.N., Tchakerian M., Xi W. and Guldin J.M., 2010. A simple stochastic weather generator for ecological modeling. Environmental Modelling and Software, 25 (10):1252-1255.

Danuso F., Della Mea V., 1994. Development and evaluation of a stochastic model for the generation of weather data. III ESA Congress, Abano, Padova, 18-22 September 1994

Danuso F., 2002. CLIMAK: a stochastic model for weather data generation. Italian Journal of Agronomy, 6 (1): 57-71.

Danuso F. 2003. SEMoLa: uno strumento per la modellazione degli agroecosistemi. Atti XXXV Convegno SIA, 16-19 September 2003, Napoli, 283-284.

Danuso F., Rocca A., Bashanova O., Ginaldi F., 2011. Una nuova versione del generatore climatico Climak, Atti Convegno AIAM, Bologna.

Doorembos J. and Pruitt W.O., 1977. Guidelines for predicting crop water requirement. FAO Irrigation and Drainage Paper n. 24. Rome.

Donatelli M., Bellocchi G., Carlini L., Colauzzi M., 2005. CLIMA: a component-based weather generator. Proc. MODSIM 2005, December 12-15, Melbourne, Australia.

Donatelli M., Bellocchi G., Habyarimana E., Bregaglio S., Confalonieri R., Baruth B., 2009. Clima: a weather generator framework. Proc. MODSIM 2009, July 13-17, Cairns, Australia.

Donatelli M. 2011. Personal communication.

Fatichi S., Ivanov V.Y. & Caporali E. (2011) Simulation of future climate scenarios with a weather generator. Advances in Water Resources 34: 448-467.

Hayhoe H.N., 2000. Improvements of stochastic weather data generators for diverse climates. Climate Research, 14: 75-87.

Jones J.W., Colwick R.F., Threadgill E.D., 1970. A simulated environmental model of temperature, evaporation, rainfall and soil moisture. ASAE Paper n. 70-404.

Keisling T.C., 1982. Calculation of the length of day. Agron. J., 77:500-505.

Larsen G.A., Pense R.B., 1982. Stochastic simulation of daily climatic data for agronomic models. Agron. J., 74: 510-514.

Matsumoto M. and Nishimura T., 1998. "Mersenne Twister: A 623-dimensionally equidistributed uniform pseudorandom number generator", 1998. ACM Trans. on Modeling and Computer Simulation, 8 (1), January pp. 3-30.

Qian B.D., Gameda S., Hayhoe H., De Jong R., and Bootsma A., 2004. Comparison of LARS-WG and AAFC-WG stochastic weather generators for diverse Canadian climates. Climate Research 26: 175-191.

Richardson C.W., 1981. Stochastic simulation of daily precipitation, temperature and solar radiation. Water Resour. Res., 17: 182-190.

Richardson C.W. and Nicks, A.D., 1990. Weather generator descriptor. In "EPIC - Erosion /productivity Impact Calculator. 1. Model documentation. USDA, Tec. Bull. 1768, Temple TX.

Semenov M.A., Brooks R.J., Barrow E.M. Richardson C.W., 1998. Comparison of WGEN and LARS-WG stochastic weather generator for diverse climates. Climate research, 10: 95-107.

Shu Geng, Penning de Vries F.W.T., Supit I., 1985. Analysis and simulation of weather variables. Part II: temperature and solar radiation. Simulation Reports CABOTT n. 5.

Tackle E.S. and Brown J.M., 1977. Note on the use of the Weibull statistics to characterize wind-speed data. Journal of applied meteorology, 17: 557-559.

Weisser D. and Foxon T.J., 2003. Implication of seasonal and diurnal variations of wind velocity for power output estimation of a turbine: a case study of Grenada. Int. J. Energy Res., 27: 1165-1179.

Estimates of sensible heat flux of heterogeneous canopy crop using different micrometeorological methods

Simona Consoli[1*], *Rita Papa*[1]

Abstract: *The paper reports on an experiment over an orange orchard to define the reliability of Surface Renewal (SR) analysis for estimating sensible heat flux, H. The orange orchard was located in Eastern Sicily (Italy) where clear skies, high summer temperatures, light winds, no rainfall and regional advection were typical weather conditions. The technique has the advantage that only requires measurement of the scalar (air temperature) at a point. High-frequency temperature traces showed ramp-like structures, and structure functions were used to determine the mean amplitude and duration of these ramps. The ramp characteristics were used to estimate H. In the study, sensible heat flux values were also obtained from the application of a simplified aerodynamic method (SAM), in which a flux density can be related to the gradient of wind speed and temperature in the atmospheric sub-layer. The reliability of SR and SAM results was evaluated through comparisons with eddy covariance measurements of H.*
The use of SR and SAM sensible heat flux values in the energy balance determination of LE can give results nearly as accurate as those obtained using eddy covariance.
Keywords: *crop water requirement, energy flux exchange, evapotranspiration, micrometeorological method.*

Riassunto: *La sperimentazione, condotta su un agrumeto adulto ubicato nella Sicilia Orientale, è stata finalizzata alla valutazione dell'affidabilità della tecnica micrometeorologica Surface Renewal (SR), utilizzata per la stima dei flussi di calore sensibile (H) scambiati dal sistema vegetazione-atmosfera. L'area in studio presenta tipiche condizioni climatiche mediterranee, caratterizzate da elevate temperature estive, moderata velocità del vento, assenza di precipitazioni estive ed avvezione regionale. La tecnica ha il vantaggio di richiedere, per la stima dei flussi di H, la misura dello scalare considerato (temperatura dell'aria) ad una sola altezza. La misura ad alta frequenza della temperatura dell'aria presenta una tipica struttura denominata "rampa", avente quali grandezze caratteristiche l'ampiezza e la durata, entrambe determinate mediante l'implementazione di "funzioni di struttura". Nello studio, le grandezze caratteristiche delle rampe di temperatura sono state utilizzate per la stima di H. I flussi di calore sensibile sono, inoltre, stati determinati mediante l'applicazione di un modello aerodinamico semplificato (SAM), nel quale la densità del flusso di H è stata messa in relazione con il gradiente di temperatura misurato a fissate altezze al di sopra della vegetazione. L'affidabilità dei metodi SR e SAM è stata, infine, confrontata con la tecnica Eddy Covariance, che consente misure dirette di H. I flussi di H, stimati mediante le tecniche SR e SAM, sono stati utilizzati per risolvere l'equazione di bilancio energetico superficiale, ottenendo come termine residuo il flusso di calore latente LE (o evapotraspirazione). Quest'ultimo è risultato confrontabile con le misure dirette di LE tramite Eddy Covariance.*

Parole chiave: *evapotraspirazione, metodi micrometeorologici, richieste idriche colturali, scambio dei flussi energetici.*

1. INTRODUCTION

The consumptive water use, or evapotranspiration (ET), can be estimated by micrometeorological methods and the energy balance equation, soil depletion techniques, or by using weighing lysimeters. Sap flow in plant trunks can be used to determine transpiration. These methods usually are expensive, difficult to operate, and some of them present problems for measurements in heterogeneous vegetation (Simmons *et al.*, 2007). Therefore, the search for accurate methods for estimating ET fluxes using low-cost, transportable and robust instrumentation is a subject of interest (Castellvì *et al.*, 2006).

The eddy covariance (EC) method is the commonly used micrometeorological technique providing direct measurements of latent heat flux. It uses a sonic anemometer to measure high-frequency vertical wind speed fluctuations about the mean and an infrared gas analyzer to measure high frequency water concentration fluctuations. The fluctuations are paired to determine the mean covariance of the wind speed and humidity fluctuations about the mean to directly estimate latent heat flux (LE). In the EC method, the

* Corresponding Author: e-mail: simona.consoli@unict.it
[1] University of Catania, Dipartimento di Gestione dei Sistemi Agroalimentari e Ambientali (DiGeSA), Catania (ITALY)
Received March 2012, accepted March 2012.

sensible heat flux is also estimated using the covariance of the fluctuations in vertical wind speed and variations in temperature about their means. While the preferred method for measuring turbulent fluxes is the EC, it is known that the closure of the surface energy balance is not guaranteed (Castellvì *et al.*, 2002; 2008). The fact that available energy does not equal the sum of the latent and sensible heat flux is commonly attributed to the lack of fetch and loss of flux by convection (Twine *et al.*, 2000; Wilson *et al.*, 2002). Additionally, the EC equipment is expensive and requires a continuous maintenance and monitoring for accurate measurements. Other energy balance approaches, such as the Bowen ratio and aerodynamic methods, have a sound theoretical basis and can be highly accurate for some surfaces under acceptable conditions. Paw U and Brunet (1991) proposed the Surface Renewal (SR) method for estimating scalar fluxes. The SR method is Lagrangian in nature and is based on the scalar conservation equation (Castellvì *et al.*, 2008). The method has been tested with air temperature data recorded over various crop canopies and it provides good estimates of sensible heat flux (H) regardless of the stability conditions and the flux direction (Paw U *et al.*, 1995; Spano *et al.*, 1997; 2000; Consoli *et al.*, 2006). The approach has the advantages that (i) requires as input only the measurement of scalar trace; (ii) involves lower costs for the experiment set-up, with respect to the EC method; (iii) operates in either the roughness or inertial sub-layers; (iv) avoids levelling, shadowing, and fetch requirements. Snyder *et al.*, (1996) and Spano *et al.*, (1997), however, have indicated the SR method currently requires an appropriate calibration factor that depends on the surface being measured (Chen *et al.*, 1997).

The aerodynamic method is another micrometeorological method used during experimental campaigns where it is necessary to characterize the soil-canopy-atmosphere continuum, and it is based on the assumption that a flux density can be related to the gradient of wind speed and temperature in the atmosphere surface layer. It starts from the logarithmic profile expression of air temperature and wind speed, corrected for atmospheric thermal stability by means of stability functions (Paulson 1970). The accuracy of the aerodynamic metod to measure H depends on the number of measurements levels of wind speed and temperature profiles.

This paper evaluates the performance of surface renewal (SR) and a semplified aerodynamic (SAM) analysis on flux estimates over orange orchard during 1 year period in an experimental site located in the Eastern Sicily (Italy). Uncalibrated surface renewal (SR) sensible heat flux (H_{SR}') values were compared against independent H_{EC} measurements obtained with an eddy covariance system, to determine a calibration factor (α) for estimating H_{EC} from H_{SR}'. The aim of this work was to evaluate alternative micrometeorological methods as reasonable accurate, low-cost and long-term procedure to obtain reliable estimate of latent heat flux (λE, or ET_c) using SR or SAM values of H and the energy balance equation.

2. METHODOLOGY

2.1 Field site experiment

The experiment was carried out over a 120 ha (37° 16' 41"N 14° 53' 01" E) orange orchard (variety navel) located in Eastern Sicily (Italy) from September 2009 to September 2010. The orchard architecture consisted of mature trees, about 3.5 m tall, with a mean leaf area index (LAI) of 4.25 m^2, PAR light interception of 100% within rows and of 50% between rows. Orange orchards were surface drip irrigated with daily frequency during May-October period. The irrigation systems included on-line labyrinth drippers, in a number of four per plant, spaced at 0.80 m, with discharge rate of 4 l/h at a pressure of 100 kPa.

There was 4 meter of distance between trunks within rows and 5.5 m between rows. The field provides an opportunity for micrometeorological studies because of the flat, homogeneous and wide site. The site is located within the agricultural context of the Catania Plain (Eastern Sicily) where clear skies, high summer temperature, light wind, no rainfall during summer and regional advection were the typical weather conditions. Regardless of the wind direction, the fetch was large because the trees were similar for the adjacent plots.

The eddy covariance (EC) technique (Aubinet *et al.* 2000) was used to simultaneously measure the mass and energy exchange flux densities over the orchard field. It encompassed a 3-dimensional sonic anemometer (CSAT3) for measuring the components of wind and a fast-responding open-path gas analyzer *LI-7500* (LI-COR, Lincoln, NE, USA) to measure carbon dioxide and latent heat flux. The EC equipment was mounted at 8 meter above the soil surface.

The net radiation (R_n) over the crop (at 8 meter from soil surface) was determined using two net radiometers (CNR 1 Kippen&Zonen). Net radiation measurements were representative of the average

mixed conditions characterizing the heterogeneous context under study.

At the plot, soil heat flux (G) was measured using a network of three soil heat flux plates (HFP01, Campbell Scientific Ltd), which were placed horizontally 0.05 meter below soil surface. Three different measurements of *G* were selected: in the trunk row (shaded area), at 1/3 distance to the adjacent row, and at 2/3 of the distance to the adjacent row. The soil heat flux was measured as the mean output of three soil heat flux plates. The gradual build up of plant matter changed the thermal properties of the upper layers. Consequently, heat storage (ΔS) was quantified in the upper layer by measuring the time rate of change in temperature. The net storage of energy (ΔS) in the soil column was determined from the temperature profile taken above each soil heat flux plate. Three probes (TCAV) were placed in the soil to sample soil temperature. The sensors were placed 0.01-0.04 m (z) below the surface; the volumetric heat capacity of the soil C_v was estimated from the volumetric fractions of minerals (V_m), organic matter (V_0) and volumetric water content (θ). Therefore, G at the surface is estimated by measuring G' at the depth of 0.05 m and the change in temperature with time of the soil layer above the heat flux plates to determine ΔS.

$$G = G' + \Delta S = G' + C_v \left(\frac{T_f - T_i}{t_f - t_i} \right) \cdot d_g \qquad (1)$$

where G' is the heat flux density measured by the plate, ΔS is the heat storage, T_f is the final temperature at time t_f, T_i is the initial temperature at time t_i (the measurement time interval was of 30 min), d_g is the depth (m) of the heat flux plates, and C_v is the volumetric heat capacity ($J \cdot m^{-3} \cdot K^{-1}$), which depends on the bulk density (ρ_b) of the soil and the volumetric water content (θ) (De Vries 1963).

A 3-D sonic anemometer (Windmaster Pro, Gill Instruments Ltd) and two fine wire thermocouples (76.2 μm diameter) were set up at 0.5 meter above the canopy top (4 meter). The SR method to estimate *H* is based on high frequency temperature measurements. When plotted, the temperature traces show ramp like characteristics, which are used to estimate heat fluxes using a conservation of energy equation (Paw U *et al.*, 1995; Snyder *et al.*, 1996; Spano *et al.*, 1997). The fine-wire thermocouples were, thus, used to measure high frequency (4 Hz) temperature fluctuations and SR estimates of *H* were computed using a structure function (Van Atta 1977) and time lags of 0.25 and 0.50 seconds for each thermocouple to determine the mean ramp-like temperature trace characteristics.

The three wind components and air temperature were recorded at 10 Hz. Wind components were rotated to force the mean vertical wind speed to zero and to align the horizontal wind speed to the mean streamwise direction (Kaimal and Finningan 1994).

Volumetric water content was measured hourly from 0.3 to 0.6 meter by using the time domain reflectometry theory (TDR) (CS 616, Campbell Scientific, Logan UT, USA). The site was also equipped with an automatic weather station to measure the values of ancillary meteorological features (i.e. solar radiation, precipitation, air temperature, relative humidity, pressure, wind speed and direction).

Air temperature and wind speed profiles were realized within the orchard in order to apply the aerodynamic analysis. Wind speed and air temperature sensors were installed at 4.5, 6.5, 8.0 and 10.0 meter above the soil surface; data were recorded at 30 minute intervals. To monitor canopy temperature and detect stress conditions onset, five infrared thermometers (IRTS-P, Apogee) were installed within the orchard.

2.2 Surface Renewal technique

Consider an air parcel travelling at a given height above the canopy. SR analysis assumes that, at some instant, the parcel suddenly moves downward into the canopy where it remains for a period of time during which it travels horizontally until the parcel is ejected upwards and replaced by another parcel sweeping in from aloft. During the connect time with the canopy, the parcel has been heated (or cooled) because of heat exchange between the air and canopy elements. When high-frequency temperature measurements are collected at fixed point, the renewal process of heated (or cooled) air parcels across a horizontal surface at height z can be visualized in the time as a regular and low frequency ramp-like pattern (asymmetric triangular shape) (Paw *et al.*, 1995) (Fig. 1). A ramp is characterized by an amplitude (a, °C) and the period (l+s, sec).

In Snyder *et al.* (2000) high frequency temperature data were processed in a datalogger to output half-hour means of the 2nd, 3rd, and 5th order moments of the time lag temperature differences. Then the moments were uploaded and analyzed to determine the amplitude (a) and the inverse ramp frequency

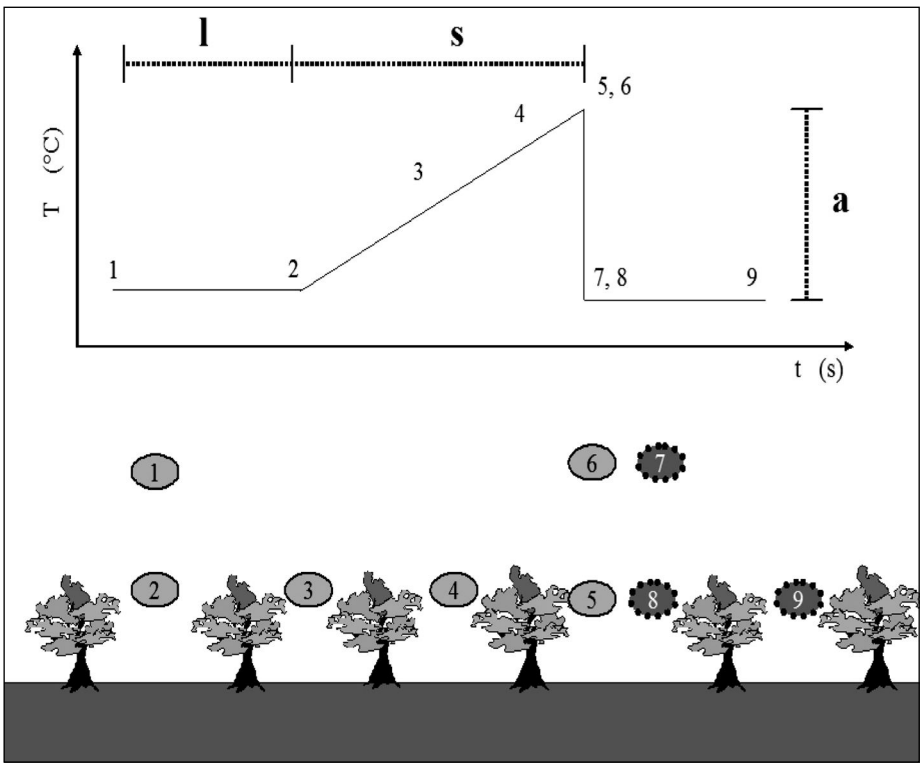

Fig. 1 - Air parcel in the renewal process.
Fig. 1 - Particella d'aria nel processo di rinnovamento.

(l+s) using the Van Atta (1977) structure function methodology.
For temperature recorded at canopy top, the surface renewal equation for sensible heat flux density H is expressed as (Paw U *et al.*, 2005):

$$H = \alpha \rho C_p \frac{a}{l+s} \cdot z \qquad (2)$$

where ρ and C_p are the density and the specific heat of dry air at constant pressure, z is the measurement height and a is a calibration factor embodying temperature variation in the canopy, initially estimated at 0.5 to account for a linear change in temperature with height. If the mean air parcel heats uniformly throughout, then a=1.
In the study sensible heat flux data from SR technique (H_{SR}) were calibrated with independent measurements of H_{EC} by the 3-D sonic anemometer located at the same fine-wire thermocouples level (4 meter). The calibration data subset was used to derive the α value of Eq. 2 by simple linear regression forced through the origin. For this regression, H_{EC} was used as the dependent variable and H_{SR} as the independent one. In this way, the regression slope was the a value looked for, used to correct H from the uncalibrated SR analysis. Calibration was made for stable and unstable cases. For stable cases, samples were split to discriminate surface cooling (R_n-G)≤0 W m^{-2} (i.e., mostly night hours), from daylight hours with (R_n-G) >0 W m^{-2} (i.e., influenced by regional advection of sensible heat flux). For calibration, the datasets selected corresponded to the central 15 days within a 3 months period. Thus, the dataset used for calibration were from day of year 75 to 90, 159 to 172 and 244 to 258, respectively for the corresponding three months period, February-April, May-July and August-October.

2.3 A simplified aerodynamic method

The sensible heat flux H is determined by the flux-gradient relationship:

$$H = -\rho C_p u^* T^* \qquad (3)$$

where u* and T* are, respectively, deduced from the wind and air temperature profile measurements. All the required correction functions for stability are described clearly and systematically by Stull (1988), Kaimal and Finningan (1994) and Arya (2001).
A simplified version of the method has been proposed by Itier (1981) and Riu (1982). In this version, the measurement of Δu and ΔT is only necessary on two levels and the used model avoids the iterative scheme imposed by the conventional functions for stability corrections (Kaimal and Finningan 1994). The method is based on the flux-

gradient relationship and the Monin-Oboukhov similarity theory. Calculation of H is dependent on atmospheric stability which is estimated by means of the Richardson number, R_i:

$$R_i = \frac{g}{T}\frac{\partial T/\partial z}{(\partial u/\partial z)^2} \quad (4)$$

where g (m s^{-2}) is the acceleration due to gravity. On the basis of R_i values, H calculation is made by four equations:

I. Moderate instability condition ($-0.3 \leq R_i \leq 0$, day situation):

$$H = K\Delta T\Delta u\left(1 - K_R\frac{\Delta T}{\Delta u^2}\right)^{3/4} \quad (5)$$

where K e K_R are coefficients depending on the position of the sensors:

$$K = \frac{-\rho C_p k^2}{\left[\ln\left(\frac{z_2}{z_1}\right)\right]^2} \quad K_R = \left(\frac{16g}{T}\right)\sqrt{z_1 z_2}\ln\left(\frac{z_2}{z_1}\right) \quad (6)$$

where k is the von Karman constant and z_1 and z_2 are the heights of the first and second sensors, respectively.

II. Very unstable condition (Ri<-0.3, day situation):

$$H = \beta\Delta T^{3/2} \quad (7)$$

with:

$$\beta = \frac{1.3\rho C_p (g/T)^{1/2}}{5.2\left[(z_1 - d)^{-1/3} - (z_2 - d)^{-1/3}\right]^{3/2}} \quad (8)$$

III. Moderate stability condition ($0 < Ri \leq 0.15$, night situation):

$$H = K\Delta T\Delta u\left(1 - \frac{\Delta T\Delta z}{6\Delta u^2}\right)^2 \quad (9)$$

IV. Very stable condition (Ri>0.15, end of clear nights):

$$H = K\Delta T\Delta u\left(1 - \frac{\Delta T\Delta z}{6\Delta u^2}\right)^2 \quad (10)$$

In the application of the simplified aerodynamic method (SAM) two elements must be underlined: (i) measurements levels z_1 and z_2 must be chosen so that z_2 is high enough to keep $(z_1 z_2)^{1/2}$ outside the roughness layer; (ii) $(z_2 - z_1)$ must be large enough to measure wind and temperature differences with sufficient accuracy. In the proposed application of the method, z_1 was posed at 4.5 meter and z_2 assumed values of 6.5, 8 and 10 meters, respectively, from the soil surface layer.

2.4 Latent heat flux estimates

When evapotranspiration is considered under the form of latent heat flux density (LE), it is worth considering all the energetic components acting above a vegetated surface, i.e. the energy balance, which can be written as:

$$LEM = R_n - G - H \quad (11)$$

where all the terms are in W m^{-2}, R_n is the net resulting from the balance of all the radiations above the crop and is directly measurable, G is the flux of heat in the soil, also directly measurable, and H is the flux of sensible heat, which was determined in the study from the application of SR, EC and SAM methodologies.

2.5 Performance indicators

Linear regression analysis, L_{RA} (slope, *s*, intercept, *int*, determination coefficient R^2) and the root mean square error, RMSE, were used to compare the sensible heat flux estimates using SR (H_{SR}) and SAM (H_{SAM}) analyses against the eddy covariance (EC) method (H_{EC}). The coefficient $D = \Sigma y/\Sigma x$ which is the sum of the flux estimates (Σy) over the sum of fluxes taken as reference (Σx), where H_{EC} is the reference data, was also determined as an evaluation parameter (Marth 1988). Because regression analysis assumes that H_{EC_8m} (the reference) is free of random sampling errors, the coefficient D was also determined as an integrated evaluation in daily, weekly, monthly, etc. time scales by averaging out errors in the half-hourly estimates (i.e., the bias is times the mean of H_{EC_8m}).

3. RESULTS AND DISCUSSION

Tab. 1 shows for each calibration period, the number of samples, N, available, the calibrated α at 4 meter (α_{4m}) for H_{SR} and the linear regression analysis (slope, *s* and intercept, *int*), R^2 and RMSE comparing H_{EC_4m} versus H_{EC_8m}.

In the paper, the estimates H values from SR and SAM were compared versus the H measured using the EC system deployed at z = 8 m, (i.e., it is the H desired to estimate LE). Fig. 2 shows the energy balance closure at 8 meter.

Case N	$\alpha_{z=4m}$	Rmse	s	int	R^2	RMSE
P: 75-90						
Unstable	0.66	61	**0.85**	**-4**	**0.94**	**35**
304	0.32	13	**0.67**	**-1**	**0.70**	**12**
Stable$^-$						
286						
P: 159-172						
Unstable	0.58	75	**0.81**	**2**	**0.86**	**49**
271	0.21	17	**0.53**	**-8**	**0.55**	**14**
Stable$^-$	0.41	14	**0.35**	**-9**	**0.23**	**21**
108						
Stable$^+$						
29						
P: 244-258						
Unstable	0.76	51	**0.89**	**2**	**0.86**	**25**
183	0.25	13	**0.42**	**-7**	**0.29**	**15**
Stable$^-$	0.38	9	**0.74**	**-3**	**0.38**	**13**
274						
Stable$^+$						
61						

+ and – denotes (Rn-G) positive and negative, respectively.

Tab. 1 - Calibration of parameter α for method SR at height z =4 m ($\alpha_{z=4m}$). In bold, the performance of H_{EC_4m} versus H_{EC_8m}. The Rmse and the *int* are in Wm^{-2}.
Tab. 1 - Calibrazione del parametro α per il metodo SR all'altezza z=4m ($\alpha_{z=4m}$). In grassetto, la performance di H_{EC_4m} rispetto a H_{EC_8m}. I valori di Rmse ed int sono espressi in Wm^{-2}.

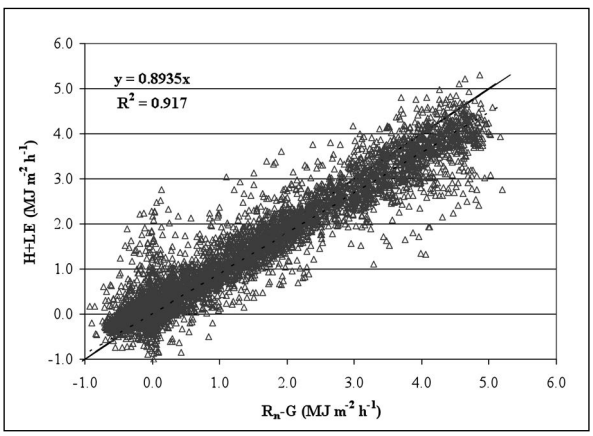

Fig. 2 - Energy balance closure at 8 meter.
Fig. 2 - Chiusura del bilancio energetico a 8 metri.

The H values estimated from SR and SAM (with z_2=10 meter) were close to H from EC method. Fig. 3 and 4 show that the hourly H_{SR} and H_{SAM} versus H_{EC} were similar for a wide range of H. When the simplified aerodynamic method (SAM) was applied with z_2 at 8 or 6.5 meter, H_{SAM} resulted quite different from H_{EC}. Most likely (z_2-z_1) wasn't large enough to measure wind and temperature differences with sufficient accuracy. In fact, when the atmospheric surface boundary layer is moderate or quite unstable, similar studies indicate that the roughness sub-layer depth mostly varies from 1 to 2

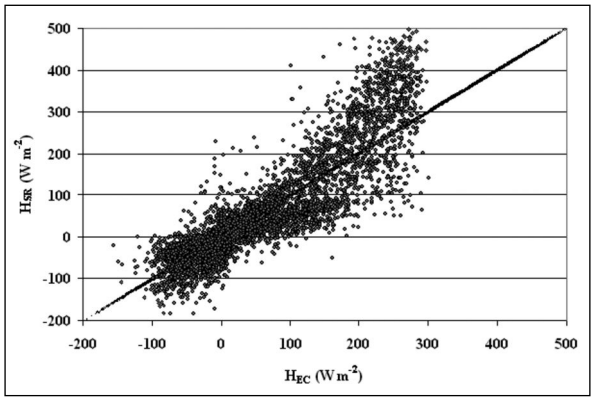

Fig. 3 - Hourly H estimates using SR analysis, H_{SR}, versus the measured using the EC method at 8 meter, H_{EC}.
Fig. 3 - Confronto tra le stime orarie di H ottenute attraverso il metodo di analisi SR, H_{SR}, ed i valori misurati utilizzando il metodo EC a 8 metri, H_{EC}.

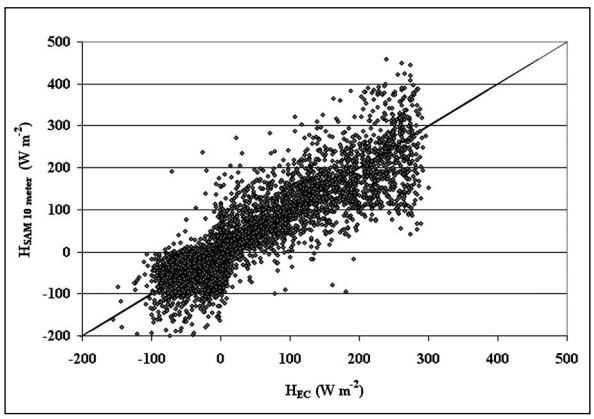

Fig. 4 - Hourly H estimates using SAM with z_2=10 meter, H_{SAM}, versus the measured using the EC method at 8 meter, H_{EC}.
Fig. 4 - Confronto tra le stime orarie di H ottenute attraverso il metodo SAM con z_2=10 metri, H_{SAM}, ed i valori misurati utilizzando il metodo EC a 8 metri, H_{EC}.

times the canopy height (Castellvì and Snyder 2009). Fig. 5 shows the frequency of z = 8 m to be above the roughness sublayer versus time (GMT) Castellvì *et al.* 2012). In general, it is shown that for hours with negative (Rn-G), the measurement height mainly remained within the inertial sub-layer. For positive (Rn-G) the roughness sublayer depth was oscillating around the upper level for about the 50% of the samples from sunrise until about two hours after noon, and late afternoon the upper level tended to remain in the inertial sublayer. Furthermore, some spurious H estimates were obtained from SAM during moderate and very stable atmospheric conditions, thus reducing the available data set for the comparison. In particular, the number of samples gathered under unstable atmospheric conditions was higher than from stable conditions.

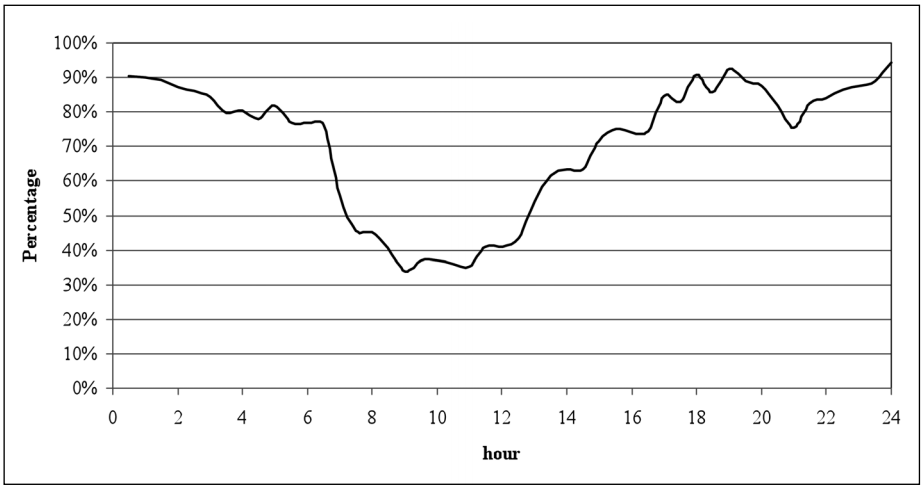

Fig. 5 - Percentage of cases when z=8 m falls above z*.
Fig. 5 - Percentuale di casi in cui z=8 m ricade al di sopra di z.*

Tab. 2 shows the results of the linear regression analysis (slope, intercept and coefficient of determination, R^2), root square mean error, RMSE, and D obtained for the analyzed data set. The largest RMSE values were obtained using the simplified aerodynamic method applied at 8 and 10 meter. In a review of experiments where the measurements were taken in the roughness sublayer, the RMSE values found to adjust surface renewal method where lower than that in Table 1 (Paw U *et al.*, 1995; 2005; Castellvì *et al.*, 2004). However these experiments are not direclty comparable because H was measured using a one dimensional sonic anemometer.

Slight underestimations by the proposed alternative methods (SR and SAM) were observed. A 3.8% underestimation was found by SR for the whole data set including both stable and unstable cases; as a result that for small fluxes the ramp amplitude was often not in accord with the sign of $H_{EC.}$ RMSE values from SR and SAM were not high. SR and SAM linear regression analyses showed slopes of, respectively, 1.12 and 0.95 very close to unit and high coefficients of determination.

For optimized drip irrigation, hourly LE estimates are desired. The best LE estimates from eq.11 are attained when all the terms are averaged hourly. A better closure may be achieved when turbulent fluxes are determined using longer block averages than half-hourly because lower frequencies are captured as well (Finningan *et al.*, 2003). However, SR is based on the analysis of organized motion near the canopy-atmosphere interface. The continuous ramp patternexhibited in the scalar trace is a canopy-scale coherent structure, which is not associated with large circulations. Therefore, the H_{SR} is best determined half-hourly. Comparisons of LE_{EC} using hourly block averages versus hourly L_{SR} and L_{SAM} (obtained from the residual energy balance method) were slightly worse than that between H values obtained from the different micrometeorological techniques. The hourly LE_{SR} and LE_{SAM} were closer to LE_{EC} mainly under unstable cases.

	H_{SR} versus H_{EC}	H_{SAM} (z_2= 10 m) versus H_{EC}	H_{SAM} (z_2= 8 m) versus H_{EC}	H_{SAM} (z_2= 6.5 m) versus H_{EC}
a	1.12	0.95	1.20	1.87
b (W m^{-2})	-5.80	-2.33	2.96	-4.58
R^2	0.80	0.77	0.63	0.75
RMSE (W m^{-2})	50.19	44.52	58.92	117.11
D	0.96	0.88	1.11	1.72

Tab. 2 - Linear regression analysis, RMSE, D, comparing the hourly H_{SR} and H_{SAM} (with different z_2) versus H_{EC} for the whole data set.
Tab. 2 - Analisi di regressione lineare, RMSE, D, relativi al confronto dei valori orari di H_{SR} e H_{SAM} (con diverso z_2) con quelli di H_{EC} per l'intero set di dati.

	H_{EC} (W m^{-2})	H_{SR} (W m^{-2})	H_{SAM} (W m^{-2})	R_N-G (W m^{-2})	LE_{EC} (W m^{-2})	LE_{SR} (W m^{-2})	LE_{SAM} (W m^{-2})	u (m s^{-1}) z_1=4.5	z_2=6.5	z_2=8	z_2=10
M	105.0	114.2	102.1	226.8	145.6	112.6	124.7	1,5	1,9	2,1	2,3
σ	92.1	125.1	96.6	182.1	102.0	107.1	119.6	1,1	1,3	1,5	1,6

Tab. 3 - Means (M) and standard deviations (σ) of the main energy fluxes and wind speed characteristics along the vertical profile. Fluxes are determined for unstable atmospheric condition cases.
Tab. 3 - Medie (M) e deviazioni standard (σ) dei principali flussi energetici e caratteristiche della velocità del vento lungo il profilo verticale. I flussi sono determinati per i casi di instabilità atmosferica.

For the unstable atmospheric conditions, Tab. 3 shows the main statistics of the estimated and measured energy fluxes. The mean wind speed values from 4.5 to 10 meters were also reported. During the irrigation season (May-October period), latent heat flux density averaged 8.5, 7.0, and 7.6 MJ m^{-2} d^{-1} for the EC, SR and SAM, respectively.
The mean (about 0.90) of daytime evaporative fraction (EF) during summer, which characterizes the partition of the energy budget at the daily time scale, varied little (0.06) based on average cloudiness. The temporal variability of the partitioning, expressed in terms of EF daily standard deviation, reached a maximum of 14%. The experiment showed that the evaporative fraction computed from flux measurements at 4 hours past sunrise tends to increase very slowly, thus to assume that the underestimation in daytime average would be not significant.
Actual crop ET (ET_a) was computed by dividing LE by the latent heat of vaporization: L = 2.45 MJ m^{-2} mm^{-1}. Generally, crop coefficients are determined by calculating the ratio $K_{co}=ET_c/ET_o$, where ET_c is the evapotranspiration of a well-watered crop. Since these orchards are well managed, it is assumed that there was little or no transpiration reducing water stress and $ET_a \approx ET_c$. Hourly variations of crop coefficient (K_{co}) values, during the monitoring period, were determined using ET_c and reference evapotranspiration (ET_o) for a short canopy (Allen *et al.*, 1998). Weather data used to calculate ET_o came from the SIAS station (the agro-meteorological service of the Sicilian region) which is located 4 km far from the site. Hourly ET_o values were summed over 24-hour periods to obtain daily ET_o.
During May-October period, average daily values of ET_c were of 3.5, 2.9 and 3.1 respectively from EC, SR and SAM, with corresponding values of the hourly crop coefficient of 0.54, 0.51, and 0.62.
H_{EC_4m} and H_{EC_8m} were rather well correlated

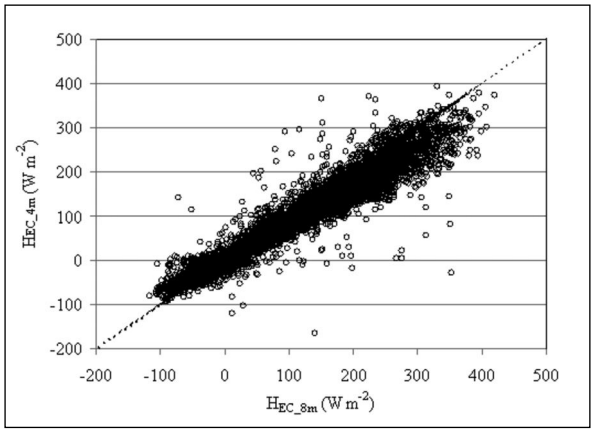

Fig. 6 - Sensible heat flux measurements using the EC method at z=4 m, H_{EC_4m} versus at z=8 m, H_{EC_8m} for all the data.
Fig. 6 - Confronto tra le misure del flusso di calore sensibile ottenute attraverso il metodo EC a z=4 m, H_{EC_4m}, e quelle a z=8 m, H_{EC_8m}, per l'intero set di dati.

(R^2=0.93) considering the different amount of small eddies (much higher close to the canopy top) that cannot be properly sampled by sonic anemometer. Fig. 6 shows H_{EC_4m} versus H_{EC_8m} for all the campaign. In general H_{EC_4m} underestimated H_{EC_8m} of 18%. For unstable cases, the a values for unequal heating was of 0.61 at 4 meter and of 0.68 at 8 meter.

CONCLUSIONS

This paper reports on an experiment in orange orchard to study the reliability of alternative micrometeorlogical techniques, such as surface renewal (SR) and a simplified aerodynamic method (SAM), for estimating sensible heat fluxes. The SAM analysis was accomplished by coupling different equations based on simple gradient flux expressions to account for atmospheric changes depending on stability or unstability conditions. H estimates using the alternative techniques were compared with H data directly measured by eddy covariance at the same site.
In general H_{SR} and H_{SAM} were similar to H_{EC}

regardless of the atmospheric stability conditions, demonstrating the potential of SR and SAM analyses as methods applicable to estimate sensible heat flux. The SAM was more sensitive to moderate and very stable atmospheric conditions, thus resulting in some spurious data.

SR technique appears in advantage with respect to SAM and EC because it may operate close to the canopy, thus minimizing fetch requirements, which make it a useful micrometeorological method where fetch requirements limit the application of other techniques.

The combination of the SR procedure and the simplified surface energy balance equation appears to be an affordable alternative to be considered for estimating water use in agriculture.

REFERENCES

Allen R.G., Pereira L.S., Raes D., Smith M., (1998). Crop evapotranspiration: Guidelines for computing crop water requirements. Irr. & Drain. Paper 56, FAO Rome.

Arya S.P., (2001). Introduction to micrometeorology. Academic Press, London, UK, 420 pp.

Aubinet M.A., Grelle A., Ibron A., (2000). Estimates of the annual net carbon and water exchange of forests: the EUROFLUX methodology. Adv. Ecol. Res. 30: 113–175.

Castellvi F., Perez P.J., Ibanez M., (2002). A method based on high frequency temperature measurements to estimate sensible heat flux avoiding the height dependence. Water Resour. Res. 38, doi:10. 1029/2001WR000486.

Castellvi F., Martinez-Cob A., Perez O., (2006). Estimating sensible and latent heat fluxes over rice using surface renewal. Agric. For. Meteorol. 139(1-2): 164-169.

Castellvi F., Snyder R.L., Baldocchi D.D., (2008). Surface energy-balance closure over rangeland grass using the eddy covariance method and surface renewal analysis. Agric. For. Meteorol. 148 (6-7): 1147-1160.

Castellvì F., Snyder R.L., (2009). On the performance of surface renewal analysis to estimate sensible heat flux over two growing rice fields under the influence of regional advection, J. Hydrol. 375: 546-553.

Chen W., Novak M.D., Blanck A., Lee X., (1997). Coherent eddies and temperature structure functions fro three contrasting surfaces - Part I: ramp model with finite microfront time. Bondary-Layer Meteorol. 66 (1-2): 65-80.

Consoli S., O'Connell N.V., Snyder R.L., (2006). Estimation of evapotranspiration of different orange sized orchard canopies using energy balance. J. Irr. and Drain. Engineer. ASCE 32(1): 2-8.

De Vries D.A., (1963). Thermal properties of soils, Physics of Plant Environment. Amsterdam, W.R. van Wijk eds. The Netherlands: North-Holland Publishing Co. pp. 210-235.

Finnigan J.J., Clements R., Malhi Y., Leuning R., Cleugh H., (2003). A revaluation of long-term flux measurement techniques. Part I: averaging and coordinate rotation, Boundary-Layer Meteorology 107: 1-48.

Itier B., (1981). Une mèthode simple pour la mésure du l'evapotranspiration réelle à l'échelle de la parcelle, Agronomie 1: 869-876.

Kaimal J.C., Finningan J.J., (1994). Atmospheric Boundary Layer Flows. Oxford Univ. press.

Marth L., (1988). Flux sampling errors for aircraft and towers, Journal of Atmospheric Ocean Technology, 15: 416-429.

Paulson C.A., (1970). The mathematical representation of wind speed and temperature profiles in the unstable atmospheric surface layer. J. Clim. Appl. Meteorol. 9: 857-861.

Paw U.K.T., Brunet Y., (1991). A surface renewal measure of sensible heat flux density. In preprints, 20th Conference on Agricultural and Forest Meteorology, September 10-13, 1991, Salt Lake City, Utah. American Meteorological Society, Boston, MA. pp. 52-53.

Paw U.K.T., Qui J., Su H.B., Watanabe T., Brunet Y., (1995). Surface renewal analysis: a new method to obtain scalar fluxes without velocity data. Agric. For. Meteorol. 74: 119-137.

Riou C., (1982). Une expression analytique du flux de chaleur sensible en conditions superadiabatiques à partir de mesures du vent et de la témperature à deux niveux. J. Rech. Atmos. 16: 15-22.

Simmons L.J., Wang J., Sammis T.W., Miller D.R., (2007). An evaluation of two inexpensive energy-balance techniques for measuring water use in flood-irrigated pecans (Carya illinoinensis). Agric. Water Manag. 88: 181-191.

Snyder R.L., Spano D., Paw U.K.T., (1996). Surface Renewal analysis for sensible and

latent heat flux density. Boundary-Layer Meteorol. 77: 249 - 266.
Snyder R.L., Bali K., Ventura F., Gomes-MacPherson H., (2000). Estimating evapotranspiration from bare soil or nearly bare soil." J. Irrig. & Drain. Eng. 126(6): 399-403.
Spano D., Snyder R.L., Duce P., Paw U.K.T., (1997). Surface renewal analysis for sensible heat flux density using structure functions. Agric. For. Meteorol. 86: 259-271.
Spano D., Snyder R.L., Duce P., Paw U.K.T., (2000). Estimating sensible and latent heat flux densities from grapevine canopies using surface renewal. Agric. Forest Meteorol. 104: 171-183.
Stull R.B., (1988). An Introduction to Boundary Layer Meteorology, Kluwer Academic Publishers.
Twine T.E., Kustas W.P., Norman J.M., Cook D.R., Houser P.R., Meyers T.P., Prueger J.H., Starks P.J., Wesely M.L., (2000). Correcting eddy-covariance flux underestimates over a grassland. Agric. For. Meteorol. 103 (3-8): 279:300.
Van Atta C.W., (1977). Effect of coherent structures on structure functions of temperature in the atmospheric boundary layer Arch. of Mech. 29: 161-171.
Wilson K., Goldstein A., Falge E., Aubinet M., Baldocchi D., Berbigier P., Bernhofer C., Ceulemans R., Dolman H., Field C., Grelle A., Ibrom A., Law B.E., Kowalski A., Meyers T., Moncrieff J., Monson R., Oechel W., Tenhumen J., Valentini R., Verma S., (2002). Energy balance closure at FLUXNET sites. Agric. For. Meteorol. 113: 223-143.